

Multi-Objective System-by-Design for *mm*-Wave Automotive Radar Antennas

P. Rosatti,⁽¹⁾ M. Salucci,⁽¹⁾ *Senior Member, IEEE*, L. Poli,⁽¹⁾ *Member, IEEE*, and A. Massa,⁽²⁾⁽¹⁾⁽³⁾
Fellow, IEEE

⁽¹⁾ *ELEDIA Research Center (ELEDIA@UniTN - University of Trento)*

DICAM - Department of Civil, Environmental, and Mechanical Engineering

Via Mesiano 77, 38123 Trento - Italy

E-mail: {*pietro.rosatti, marco.salucci, lorenzo.poli, andrea.massa*}@unitn.it

Website: www.eledia.org/eledia-unitn

⁽²⁾ *ELEDIA Research Center (ELEDIA@UESTC - UESTC)*

School of Electronic Engineering, Chengdu 611731 - China

E-mail: *andrea.massa@uestc.edu.cn*

Website: www.eledia.org/eledia-uestc

⁽³⁾ *ELEDIA Research Center (ELEDIA@TSINGHUA - Tsinghua University)*

30 Shuangqing Rd, 100084 Haidian, Beijing - China

E-mail: *andrea.massa@tsinghua.edu.cn*

Website: www.eledia.org/eledia-tsinghua

This work has been submitted to the IEEE for possible publication. Copyright may be transferred without notice, after which this version may no longer be accessible.

Multi-Objective System-by-Design for *mm*-Wave Automotive Radar Antennas

P. Rosatti, M. Salucci, L. Poli, and A. Massa

Abstract

The computationally-efficient solution of multi-objective optimization problems (*MOPs*) arising in the design of modern electromagnetic (*EM*) microwave devices is addressed. Towards this end, a novel System-by-Design (*SbD*) method is developed to effectively explore the solution space and to provide the decision maker with a set of optimal trade-off solutions minimizing multiple and (generally) contrasting objectives. The proposed *MO-SbD* method proves a high computational efficiency, with a remarkable time saving with respect to a competitive state-of-the-art *MOP* solution strategy, thanks to the “smart” integration of evolutionary-inspired concepts and operators with artificial intelligence (*AI*) and machine learning (*ML*) techniques. Representative numerical results are reported to provide the interested users with useful insights and guidelines on the proposed optimization method as well as to assess its effectiveness in designing *mm*-wave automotive radar antennas.

Key words: Microwave Design, Radar Antennas, Evolutionary Algorithms (*EAs*), Artificial Intelligence (*AI*), Machine Learning (*ML*), Multi-Objective Optimization Problem (*MOP*), System-by-Design (*SbD*).

1 Introduction and Motivation

The design of modern high-performance microwave devices such as filters [1], directional couplers [2], and antennas [3], generally involves a number of challenging and (sometimes) contrasting requirements on their electromagnetic (*EM*) behavior along with tight geometrical, weight, and cost constraints [4]. Such a synthesis problem is often formulated as a single-objective optimization problem (*SOP*) whose solution is the global minimum of a cost function that quantifies the mismatch between the *EM*/structural features of the synthesized device and the user-defined objectives. Several and effective solution strategies for solving *SOPs* have been presented in the scientific literature based on deterministic [5] as well as stochastic [4][6]-[8] optimization algorithms. However, since conflicting requirements are typically at hand, the arising *SOP* solution turns out to be only a particular trade-off among all the optimization targets. Otherwise, a set of optimal compromise solutions belonging to the so-called Pareto Front (*PF*) can be obtained by natively addressing the design process as a multi-objective optimization problem (*MOP*) [9]-[12]. This approach allows the designer to select the most suitable design that fulfils a specific application [10] or that features other profitable properties.

Regardless of the single- or multi-objective formulation, full-wave (*FW*) *EM* software are usually used to accurately predict the *EM* behavior of each trial design/solution [4]. Indeed, more and more reliable and precise computational tools are nowadays available [13]-[15] for the analysis of complex *EM* devices. Because of the reliability in modeling non-linear and coupling *EM* phenomena, which are generally neglected or approximated by simplified analytical approaches [16][17], they play a key-role in the study of modern microwave devices.

However, the integration of *FW* solvers in iterative optimization loops (e.g., evolutionary-algorithm (*EA*) optimizations [4][6]) is not straightforward due to the high computational burden. To counteract such an issue, significant efforts have been devoted and the proposed approaches can be classified according to the following countermeasures: (i) the exploitation of the *a-priori* knowledge on the solution through model-based approaches [18], (ii) the reduction of the dimensionality of the solution space by looking for “smart” definitions of the unknowns/degrees-of-freedom (*DoFs*) [19], (iii) a suitable initialization of the optimization process [20], and (iv) the reduction of the *CPU* time for the evaluation of the “fitness” of a

trial solution to the design objectives by means of space mapping strategies [21][22] or artificial intelligence (*AI*) and machine learning (*ML*) methods [23]-[27].

As for this latter framework, *ML* techniques based on the Learning-by-Examples (*LBE*) [28] theory that also exploit complex Deep Learning (*DL*) [29] architectures are recently gaining an increasing attention from both the scientific community and the industrial one. As a matter of fact, computationally-efficient surrogate models (*SMs*), which are able to accurately predict complex *EM* dynamics [30]-[37], can be derived starting from a training set of input/output (*I/O*) examples computed with the *FW* solver.

Based on the “interactive collaboration” between *EAs* and *LBE* methods, effective and efficient techniques for the synthesis of *EM* devices have been recently proposed according to the so-called System-by-Design (*SbD*) paradigm, which is defined as the “*task-oriented design, definition, and integration of system components to yield EM devices with user-desired performance having the minimum costs, the maximum scalability, and suitable reconfigurability properties*” [38]. The potential and the flexibility of such an approach have been demonstrated in the design of a plethora of devices including wide-angle impedance layers (*WAIMs*) [39], metamaterial lenses [40], holographic *EM* skins [41], polarizers [42], nano-structures [12], reflectarrays [43], airborne radomes [19], *5G* arrays [38], time modulated arrays [38], and automotive radar antennas [38]. However, to the best of the authors’ knowledge, *SO-SbD* methods have been proposed so far mainly without exploring the pros & cons of *MO* implementations.

Towards this end, this paper proposes a new *SbD*-based technique for the *AI*-driven solution of complex *EM* syntheses formulated as *MOPs*. From a methodological point of view, the main novelties of this work over the existing literature can be summarized as follows: (i) the integration of evolutionary-inspired concepts and operators within a new *MO-SbD* solution scheme that adaptively exploits a *ML*-based *SM* to accurately predict the “fitness” of each guess solution to the design problem at hand, (ii) the derivation of a new set of “*SbD*-dominance” criteria that allows a fruitful exploitation of the available information on the reliability index of the *SM* predictions, (iii) the implementation of a reinforced learning (*RL*) strategy to improve the accuracy of the *SM* during the *SbD* optimization loop, and (iv) the customization of the *MO-SbD* scheme to the synthesis of *mm*-wave automotive radar antennas [44].

The paper is organized as follows. Section 2 gives the mathematical formulation of the *SbD-MOP*. The description of the proposed *MO-SbD* is detailed in Sect. 3 along with its customization to the synthesis problem of designing *mm*-wave antennas for automotive radars (Sect. 3.1). The assessment of the *MO-SbD* method is carried out by first considering standard *MOP* benchmark functions (Sect. 4.1) to derive some general insights on its performance as well as useful guidelines for its application to specific applicative problems. Successively, Section 4.2 is devoted to assess the effectiveness and the computational efficiency of the *MO-SbD* in synthesizing *mm*-wave antennas for automotive radars. Finally, some conclusions and final remarks are drawn (Sect. 5).

2 Mathematical Formulation

Let K be the dimensionality of the solution space, \mathbb{R}^K , of a *MO* design problem, $\underline{\Omega}$ being a generic element of \mathbb{R}^K ($\underline{\Omega} \triangleq \{\Omega_k; k = 1, \dots, K\}$), aimed at determining the set \mathbf{A} of A ($A > 1$) Pareto-optimal trade-off solutions, $\mathbf{A} \triangleq \{\underline{\Omega}^{(a)}; a = 1, \dots, A\}$, that fulfils Q ($Q > 1$) user-defined objectives coded into the cost function vector $\underline{\Phi}$ ($\underline{\Phi}(\underline{\Omega}) \triangleq [\Phi_q(\underline{\Omega}); q = 1, \dots, Q]$, $\underline{\Phi}(\underline{\Omega}) \in \mathbb{R}^Q$).

According to the reference *MOP* literature [45][46][50], \mathbf{A} is composed by the Pareto Front (*PF*) of all *non-dominated* solutions spanning the K -dimensional search space \mathbb{R}^K , the dominance of one solution, $\underline{\Omega}^{(1)}$, over another one, $\underline{\Omega}^{(2)} \neq \underline{\Omega}^{(1)}$ (i.e., $\underline{\Omega}^{(1)} \prec \underline{\Omega}^{(2)}$) being mathematically stated as follows (Fig. 1)

$$\begin{cases} \Phi_p(\underline{\Omega}^{(1)}) < \Phi_p(\underline{\Omega}^{(2)}) & p \in \{1, \dots, Q\} \\ \Phi_q(\underline{\Omega}^{(1)}) \leq \Phi_q(\underline{\Omega}^{(2)}) & q = 1, \dots, Q; q \neq p. \end{cases} \quad (1)$$

However, because of the continuous/real nature of the Q components of $\underline{\Phi}$, the number of entries of \mathbf{A} is infinite ($A \rightarrow \infty$) and the resulting optimization task turns out to be unfeasible [46][50].

In practical scenarios, it is thus convenient to look for an alternative/approximated definition of \mathbf{A} that complies with the following assumptions: (a) the number of entries of the *PF*, A , is finite (i.e., \mathbf{A} is a bounded set) and (b) these A solutions are uniformly spread in the solution

space \mathbb{R}^K so that they are representative of all possible non-dominated solutions that comply with (1). Towards this end, the concept of ε -dominance is exploited. Accordingly, $\underline{\Omega}^{(1)}$ is said to ε -dominate $\underline{\Omega}^{(2)}$ (i.e., $\underline{\Omega}^{(1)} \prec_\varepsilon \underline{\Omega}^{(2)}$) if one of the following conditions holds true (Fig. 1) [46][50]

$$\left\{ \begin{array}{l} \left\lfloor \frac{\Phi_p(\underline{\Omega}^{(1)})}{\varepsilon_p} \right\rfloor < \left\lfloor \frac{\Phi_p(\underline{\Omega}^{(2)})}{\varepsilon_p} \right\rfloor \quad p \in \{1, \dots, Q\} \\ \left\lfloor \frac{\Phi_q(\underline{\Omega}^{(1)})}{\varepsilon_q} \right\rfloor \leq \left\lfloor \frac{\Phi_q(\underline{\Omega}^{(2)})}{\varepsilon_q} \right\rfloor \quad q = 1, \dots, Q; q \neq p \end{array} \right. \quad (2)$$

or

$$\left\{ \begin{array}{l} \left\lfloor \frac{\Phi_q(\underline{\Omega}^{(1)})}{\varepsilon_q} \right\rfloor = \left\lfloor \frac{\Phi_q(\underline{\Omega}^{(2)})}{\varepsilon_q} \right\rfloor \quad q = 1, \dots, Q \\ d_\varepsilon(\underline{\Omega}^{(1)}) < d_\varepsilon(\underline{\Omega}^{(2)}) \end{array} \right. \quad (3)$$

In (2), which is the “quantized” counterpart of (1), and (3), $\lfloor \cdot \rfloor$ is the integer floor function, while $d_\varepsilon(\underline{\Omega})$ is the Euclidean distance between $\underline{\Phi}(\underline{\Omega})$ and its “ ε -quantized” version, $\widehat{\underline{\Phi}}(\underline{\Omega})$ [$\widehat{\underline{\Phi}}(\underline{\Omega}) \triangleq [\widehat{\Phi}_q(\underline{\Omega}); q = 1, \dots, Q]$ being $\widehat{\Phi}_q(\underline{\Omega}) \triangleq \left\lfloor \frac{\Phi_q(\underline{\Omega})}{\varepsilon_q} \right\rfloor \times \varepsilon_q$] (Fig. 1)

$$d_\varepsilon(\underline{\Omega}) = \sqrt{\sum_{q=1}^Q \left[\Phi_q(\underline{\Omega}) - \widehat{\Phi}_q(\underline{\Omega}) \right]^2}. \quad (4)$$

Moreover, $\underline{\varepsilon}$ is the set of Q user-defined real values ($\underline{\varepsilon} \triangleq \{\varepsilon_q > 0; q = 1, \dots, Q\}$) that allows the designer to *a-priori* control the accuracy of the approximation of the ideal *PF*. A large value of its q -th ($q = 1, \dots, Q$) entry, ε_q , results in a coarser representation of the *PF* along the q -th objective, and vice-versa.

An illustrative example of both dominance conditions, (1) and (2)(3), is shown in Fig. 1. According to (1), it turns out that $\underline{\Omega}^{(1)} \prec \underline{\Omega}^{(3)}$ and $\underline{\Omega}^{(2)} \prec \underline{\Omega}^{(3)}$, but $\underline{\Omega}^{(1)} \not\prec \underline{\Omega}^{(2)}$ and $\underline{\Omega}^{(2)} \not\prec \underline{\Omega}^{(1)}$ (i.e., $\underline{\Omega}^{(1)}$ and $\underline{\Omega}^{(2)}$ are two non-dominated solutions). Otherwise, the solution $\underline{\Omega}^{(1)}$ ε -dominates both $\underline{\Omega}^{(2)}$ and $\underline{\Omega}^{(3)}$ (i.e., $\underline{\Omega}^{(1)} \prec_\varepsilon \underline{\Omega}^{(2)}$ and $\underline{\Omega}^{(1)} \prec_\varepsilon \underline{\Omega}^{(3)}$) according to (3), while $\underline{\Omega}^{(2)} \prec_\varepsilon \underline{\Omega}^{(3)}$.

Within the ε -dominance framework, the statement of the *MO* problem at hand can be then phrased as follows:

ε -MOP - Given a set of Q objectives, $\underline{\Phi}$, and defined the accuracy vector $\underline{\varepsilon}$, find the “optimal” *PF* of A^{opt} ($A^{opt} > 1$) non- ε -dominated solutions, \mathbf{A}^{opt} ,

$$\mathbf{A}^{opt} = \left\{ \left[\underline{\Omega}^{(a)} : \nexists b \neq a \rightarrow \underline{\Omega}^{(b)} \prec_\varepsilon \underline{\Omega}^{(a)} \right]; a, b = 1, \dots, A^{opt} \right\}, \quad (5)$$

that includes the global optimum $\underline{\Omega}^{opt}$ ($\underline{\Omega}^{opt} \in \mathbf{A}^{opt}$), $\underline{\Omega}^{opt} = \arg \{ \min_{\underline{\Omega}} [\Phi_q(\underline{\Omega}); q = 1, \dots, Q] \}$.

3 *MO-SbD* Solution Method

In order to solve the ε -*MOP* with high computational efficiency, the problem at hand is recast within the *SbD* framework as follows

SbD-MOP - Iteratively (i being the iteration index, $i = 1, \dots, I$) generate a sequence of *PFs* $\{\mathbf{A}_i; i = 0, \dots, I\}$, that converges to the optimal one \mathbf{A}^{opt} ($\mathbf{A}^{SbD} \rightarrow \mathbf{A}^{opt}$, $\mathbf{A}^{SbD} = \mathbf{A}_i \big|_{i=I_{SbD}}$, I_{SbD} being the convergence iteration) in an overall computation time Δt^{SbD} fulfilling the condition

$$\Delta t^{SbD} \ll \Delta t^{StD}, \quad (6)$$

Δt^{StD} being the time needed by a standard optimization method to reach the same *SbD* convergence condition, which is defined as

$$\Phi_q(\underline{\Omega}^{SbD}) \leq \zeta_q \quad q = 1, \dots, Q \quad (7)$$

where $\underline{\Omega}^{SbD} \in \mathbf{A}^{SbD}$ and ζ_q is the convergence threshold for the q -th ($q = 1, \dots, Q$) objective.

This latter formulation is then addressed with an innovative synthesis strategy leveraging on the “interactive collaboration” between evolutionary-inspired operators drawn from the ε -*MOEA* algorithm [46] (referred to as the “*StD*” method in the following) and *AI* techniques.

In the following, the discussion on the *SbD* implementation will focus on three main items: (1) the *AI*-based mechanisms for dealing with a faithful, but also computationally efficient, prediction of the *EM* behavior of each guess design and, in turn, the estimation of its fitness to the problem at hand [i.e., $\underline{\Phi}(\underline{\Omega})$]; (2) the multiple-agent strategy for sampling the solution space; (3) the work-flow of the algorithmic implementation of the *MO-SbD*.

As for (1), let us observe that the overall computational cost of the synthesis based on a standard

iterative optimization is equal to

$$\Delta t^{StD} = C_{FW}^{StD} \times \Delta t_{FW} \quad (8)$$

where Δt_{FW} is the average time for evaluating/computing the Q objectives/cost-function-terms associated to any trial guess solution $\underline{\Omega}$, $\{\Phi_q(\underline{\Omega}); q = 1, \dots, Q\}$, and $C_{FW}^{StD} = P + I$ is the total number of FW calls during the iterative multi-agent process, P being the population of agents/trial solutions. Thus, the computational goal of a SbD -based design (6) can be yielded by alternatively or (better) simultaneously acting on both factors in (8).

For instance, a recent trend is that of reducing the number of computationally-expensive FW calls (i.e., $C_{FW}^{SbD} \ll C_{FW}^{StD}$) by exploiting a fast surrogate model (SM) to predict the fitness value, $\underline{\Phi}(\underline{\Omega})$, of the remaining ($C_{FW}^{StD} - C_{FW}^{SbD}$) solutions (i.e., $\Delta t_{SM} \ll \Delta t_{FW}$). According to this guideline, a SM based on the Ordinary Kriging (OK) LBE technique [47][48][49] is built at each i -th ($i = 1, \dots, I$) SbD iteration, $\mathcal{F}_i\{\underline{\Omega}\}$, starting from the information learned from a training set \mathbf{T}_i of T_i I/O pairs

$$\mathbf{T}_i = \left\{ \left[\underline{\Omega}_i^{(t)}, \underline{\Phi}(\underline{\Omega}_i^{(t)}) \right]; t = 1, \dots, T_i \right\}. \quad (9)$$

Such a methodological choice is motivated by the solid mathematical background of the OK theory that allows the arising SM to output deterministic predictions, $\tilde{\underline{\Phi}}(\underline{\Omega})$, which interpolate the (FW -computed) I/O samples of the corresponding training set, \mathbf{T} [i.e., $\tilde{\underline{\Phi}}(\underline{\Omega}) \triangleq \tilde{\underline{\Phi}}(\underline{\Omega} | \mathbf{T})$]. Moreover, the by-product of using an OK -based predictor is the availability of a “reliability index” for every fitness prediction [47][48][49], $\underline{\delta}(\underline{\Omega})$ [$\underline{\delta}(\underline{\Omega}) \triangleq \underline{\delta}(\underline{\Omega} | \mathbf{T})$], whose q -th ($q = 1, \dots, Q$) entry, $\delta_q(\underline{\Omega})$ [$\delta_q(\underline{\Omega}) \triangleq \delta_q(\underline{\Omega} | \mathbf{T})$], is given by $\delta_q(\underline{\Omega}) = \sqrt{\eta_q(\underline{\Omega})}$, $\eta_q(\underline{\Omega})$ being the estimated mean squared error (MSE) of the OK prediction, $\tilde{\Phi}_q(\underline{\Omega})$, in approximating the corresponding actual value, $\Phi_q(\underline{\Omega})$ [47][48]. Quantitatively, a smaller value of $\delta_q(\underline{\Omega})$ means a higher level of reliability of the prediction [i.e., $\tilde{\Phi}_q(\underline{\Omega}) \approx \Phi_q(\underline{\Omega})$], and vice-versa ⁽¹⁾ [47][48][49].

By exploiting the information on the “reliability” of the OK predictions, the “confidence hyper-volume” of a prediction $\tilde{\underline{\Phi}}(\underline{\Omega})$, $\mathcal{V}_{\tilde{\underline{\Phi}}}$, is defined as the Q -dimensional region with the highest

⁽¹⁾The OK prediction is faithful [i.e., $\tilde{\Phi}_q(\underline{\Omega}) = \Phi_q(\underline{\Omega})$, $q = 1, \dots, Q$] with null uncertainty [i.e., $\delta_q(\underline{\Omega}) = 0$, $q = 1, \dots, Q$] if $\underline{\Omega}$ coincides with one training sample [47] (i.e., $\underline{\Omega} \in \mathbf{T}$).

probability of containing the actual value $\underline{\Phi}(\underline{\Omega})$ (Fig. 2)

$$\mathcal{V}_{\tilde{\Phi}} = \left\{ \mathcal{L}_q(\underline{\Omega}) \leq \tilde{\Phi}_q(\underline{\Omega}) \leq \mathcal{U}_q(\underline{\Omega}); q = 1, \dots, Q \right\}. \quad (10)$$

where $\mathcal{L}_q(\underline{\Omega})$ and $\mathcal{U}_q(\underline{\Omega})$ are the lower and the upper confidence bounds of the *OK* prediction, $\tilde{\Phi}_q(\underline{\Omega})$ ($q = 1, \dots, Q$): $\mathcal{L}_q(\underline{\Omega}) = \tilde{\Phi}_q(\underline{\Omega}) - \delta_q(\underline{\Omega})$ and $\mathcal{U}_q(\underline{\Omega}) = \tilde{\Phi}_q(\underline{\Omega}) + \delta_q(\underline{\Omega})$.

Concerning the sampling of the solution space (2) and similarly to the *StD* method [46], the proposed *SbD* -based strategy generates ($i = 0$) and evolves ($i = 1, \dots, I$) both a variable-size *PF*, \mathbf{A}_i , of A_i solutions ($\mathbf{A}_i = \left\{ \underline{\Omega}_i^{(a)}; a = 1, \dots, A_i \right\}$) and a fixed-size population, \mathbf{P}_i , of P individuals ($\mathbf{P}_i = \left\{ \underline{\Omega}_i^{(p)}; p = 1, \dots, P \right\}$). While the *PF* is updated exclusively with *FW*-evaluated individuals to guarantee the unambiguous knowledge of the best trade-off solutions, a more sophisticated evolution mechanism, which involves both *FW*-simulated and *SM*-predicted individuals, is used for evolving the population.

More specifically, the concept of *SbD-dominance* (i.e., $\underline{\Omega}^{(1)} \prec_{SbD} \underline{\Omega}^{(2)}$) between any pair of solutions $\underline{\Omega}^{(1)}$ and $\underline{\Omega}^{(2)}$ evaluated either with the *FW* solver or with the *SM* is introduced. It is based on the following rules: (i) an individual whose objectives have been simulated is preferred to a predicted one because of its higher trustworthiness; (ii) a simulated individual is *SbD*-dominated by a predicted one only if taking into account the corresponding confidence hyper-volume. Mathematically, such guidelines are coded into the relations in Tab. I that are also pictorially illustrated in Fig. 3 ($Q = 2$). As a representative example, let us consider the case reported in Fig. 3(c) where $\underline{\Omega}^{(1)}$ is predicted and $\underline{\Omega}^{(2)}$ is simulated. It turns out that $\underline{\Omega}^{(1)} \prec_{SbD} \underline{\Omega}^{(2)}$ because $\underline{\Omega}^{(1)}$ would dominate $\underline{\Omega}^{(2)}$ even in the “worst case” when $\underline{\Phi}(\underline{\Omega}^{(1)}) = \underline{\mathcal{U}}(\underline{\Omega}^{(1)})$.

To adaptively increase the accuracy of the predictor [$\tilde{\Phi}_i(\underline{\Omega}) \rightarrow \underline{\Phi}(\underline{\Omega})$, $i = 1, \dots, I$], while the *SbD* minimization process converges towards the optimal *PF* ($i \rightarrow I_{SbD}$), a *RL* strategy is applied to progressively update the *SM* each time a new individual is elected for being evaluated with the *FW* solver. It is worth pointing out that the designer has the full control of the total time of the *SbD* optimization, Δt^{SbD} , since the number of *RL FW* calls is *a-priori* limited to $T_{RL} \leq T_{RL}^{\max}$, T_{RL}^{\max} being a user-defined maximum value. By integrating the *AI*-based mechanisms for predicting the *EM* behavior of a guess design (I) and the strategy for sampling the solution space with evolutionary-inspired operators [46] (2), the work-flow of the *MO-SbD* in Fig. 4 consists

of two phases performed in the following chronological order: (1.) *Initialization* ($i = 0$) and (2.) *Iterative Loop* ($i = 1, \dots, I$). More in detail,

(1.) Initialization ($i = 0$)

- Set $T_{RL} = 0$. Build an initial training set \mathbf{T}_0 of T_0 *I/O* pairs ($\mathbf{T}_0 = \{ [\underline{\Omega}_0^{(t)}, \underline{\Phi}(\underline{\Omega}_0^{(t)})] ; t = 1, \dots, T_0 \}$) where the set of solutions $\{ \underline{\Omega}_0^{(t)} ; t = 1, \dots, T_0 \}$ is generated by means of the Latin Hypercube Sampling (*LHS*) method [38];
- Train the initial *SM*, $\mathcal{F}_0 \{ \underline{\Omega} \}$, with \mathbf{T}_0 ;
- Initialize the *PF* \mathbf{A}_0 ($\mathbf{A}_0 = \{ \underline{\Omega}_0^{(a)} ; a = 1, \dots, A_0 \}$, $\mathbf{A}_0 \subseteq \mathbf{T}_0$, $A_0 \leq T_0$) by applying the operator $\mathcal{N}_\varepsilon \{ \mathbf{G} \}$, which extracts all $G' \leq G$ non- ε -dominated solutions within a generic set \mathbf{G} of G solutions ($\mathbf{G} = \{ \underline{\Omega}^{(g)} ; g = 1, \dots, G \}$)

$$\mathcal{N}_\varepsilon \{ \mathbf{G} \} = \left\{ \left[\underline{\Omega}^{(h)} \in \mathbf{G} : \nexists g \in (g = 1, \dots, G) \rightarrow \underline{\Omega}^{(g)} \prec_\varepsilon \underline{\Omega}^{(h)} \right] ; h = 1, \dots, G' \right\}, \quad (11)$$

to \mathbf{T}_0 ($\mathbf{A}_0 = \mathcal{N}_\varepsilon \{ \underline{\Omega}_0^{(t)} ; t = 1, \dots, T_0 \}$);

- Choose P individuals of the initial population, $\mathbf{P}_0 = \{ \underline{\Omega}_0^{(p)} ; p = 1, \dots, P \}$, according to the following rule

$$\underline{\Omega}_0^{(p)} = \begin{cases} \underline{\Omega}_0^{(a)} \Big|_{a=p} & \text{if } p \leq \min(P, A_0) \\ \mathcal{R} \{ \underline{\Omega}_0^{(t)} ; t = 1, \dots, T_0 \} & \text{if } P > A_0 \end{cases} \quad (12)$$

($p = 1, \dots, P$), $\mathcal{R} \{ \mathbf{G} \}$ being the operator that randomly extracts one entry of \mathbf{G} [i.e., $\mathcal{R} \{ \mathbf{G} \} = \underline{\Omega}^{(r)} \in \mathbf{G}$, $r = \text{rand}(1, \dots, G)$];

(2.) Iterative Loop ($i = 1, \dots, I$)

- Generate a new solution $\underline{\Omega}_i^{(\mathcal{M})}$ by applying the following sequence of evolutionary-based operations
 - *Selection* - Randomly pick one solution from the i -th *PF*, $\underline{\Omega}_i^{(\mathcal{R})} = \mathcal{R} \{ \mathbf{A}_i \}$, and one non-dominated solution from the current population, $\underline{\Omega}_i^{(\mathcal{N})} = \mathcal{R} \{ \mathcal{N} \{ \mathbf{P}_i \} \}$,

- $\mathcal{N}\{\mathbf{G}\}$ being, analogously to (11), the operator that extracts all $G' \leq G$ (standard) non-dominated (1) solutions within a generic set \mathbf{G} of G solutions ($\mathbf{G} = \{\underline{\Omega}^{(g)}; g = 1, \dots, G\}$);
- *Crossover* - Apply the simulated binary crossover (*SBX*) recombination operator $\mathcal{X}\{\cdot\}$ [51] to generate a new individual: $\underline{\Omega}_i^{(\mathcal{X})} = \mathcal{X}\{\underline{\Omega}_i^{(\mathcal{R})}, \underline{\Omega}_i^{(\mathcal{N})}\}$;
 - *Mutation* - Determine the final offspring $\underline{\Omega}_i^{(\mathcal{M})}$ by applying the polynomial mutation operator $\mathcal{M}\{\cdot\}$ [52] to $\underline{\Omega}_i^{(\mathcal{X})}$: $\underline{\Omega}_i^{(\mathcal{M})} = \mathcal{M}\{\underline{\Omega}_i^{(\mathcal{X})}\}$;
- Input $\underline{\Omega}_i^{(\mathcal{M})}$ into the $(i - 1)$ -th *SM*, $\mathcal{F}_{i-1}\{\cdot\}$, to let it predict the objectives vector, $\tilde{\Phi}_{i-1}(\underline{\Omega}_i^{(\mathcal{M})})$, and the corresponding confidence levels, $\tilde{\delta}_{i-1}(\underline{\Omega}_i^{(\mathcal{M})})$;
 - Verify whether $\underline{\Omega}_i^{(\mathcal{M})}$ is ε -dominated by any of the A_{i-1} solutions belonging to the *PF* \mathbf{A}_{i-1} at the $(i - 1)$ -th iteration. To reduce the computational cost, each a -th ($a = 1, \dots, A_{i-1}$) ε -dominance check (2)(3) is performed by replacing the unknown actual objectives of $\underline{\Omega}_i^{(\mathcal{M})}$ [i.e., $\Phi(\underline{\Omega}_i^{(\mathcal{M})})$] with their predictions, $\tilde{\Phi}_{i-1}(\underline{\Omega}_i^{(\mathcal{M})})$. Finally, if $\underline{\Omega}_i^{(\mathcal{M})}$ is non- ε -dominated (i.e., $\nexists a \in \{1, \dots, A_{i-1}\}$ such that $\underline{\Omega}_{i-1}^{(a)} \prec_{\varepsilon} \underline{\Omega}_i^{(\mathcal{M})}$), then compute $\Phi(\underline{\Omega}_i^{(\mathcal{M})})$ with the *FW* solver, else let $\mathcal{F}_i\{\cdot\} \leftarrow \mathcal{F}_{i-1}\{\cdot\}$, $T_i \leftarrow T_{i-1}$, $\mathbf{T}_i \leftarrow \mathbf{T}_{i-1}$, and jump (avoid) the following step concerned with the *RL*;
 - Reinforce the training set \mathbf{T}_{i-1} by adding the new I/O training sample $\{\underline{\Omega}_i^{(\mathcal{M})}, \Phi(\underline{\Omega}_i^{(\mathcal{M})})\}$ (i.e., $\mathbf{T}_i = \mathbf{T}_{i-1} \cup \{\underline{\Omega}_i^{(\mathcal{M})}, \Phi(\underline{\Omega}_i^{(\mathcal{M})})\}$) and increase the indexes T_{RL} and T_i [i.e., $T_{RL} \leftarrow (T_{RL} + 1)$ and $T_i \leftarrow (T_{i-1} + 1)$]. Update the *SM*, $\mathcal{F}_i\{\underline{\Omega}\}$, with \mathbf{T}_i ;
 - Update the *PF* ($\mathbf{A}_i \leftarrow \mathbf{A}_{i-1}$) by applying the operator $\mathcal{N}_{\varepsilon}$ to the set $\{\underline{\Omega}_i^{(\mathcal{M})}, \mathbf{A}_{i-1}\}$ (i.e., $\mathbf{A}_i = \mathcal{N}_{\varepsilon}\{\underline{\Omega}_i^{(\mathcal{M})}, \mathbf{A}_{i-1}\}$);
 - Derive from \mathbf{P}_{i-1} the two complementary subsets \mathbf{P}_{i-1}^{pred} and \mathbf{P}_{i-1}^{sim} ($\mathbf{P}_{i-1} = \mathbf{P}_{i-1}^{pred} \cup \mathbf{P}_{i-1}^{sim}$) that contain all the individuals with predicted or simulated objectives, respectively. By exploiting the *SbD* updating rules (Tab. II), decide whether the new individual $\underline{\Omega}_i^{(\mathcal{M})}$ should be included in the new population \mathbf{P}_i , by substituting one properly-chosen individual of \mathbf{P}_{i-1} , or discarded (i.e., $\mathbf{P}_i \leftarrow \mathbf{P}_{i-1}$ - Tab. II) according to the *SbD*-dominance rules in Tab. I;

- Stop the iterative process and set $i = I_{SbD}$ if \mathbf{A}_i fulfils the stationarity condition

$$\sqrt{\frac{1}{W} \sum_{w=0}^{W-1} [\Gamma(\mathbf{A}_{i-w}) - \bar{\Gamma}_i]^2} \leq \gamma \quad (13)$$

over a window of W iterations, γ , $\Gamma(\mathbf{A}_{i-w})$, and $\bar{\Gamma}_i$ being a user-defined threshold, the maximum crowding distance at the $(i-w)$ -th iteration, and its average over the iteration window, respectively (see Appendix I) [53] or if the maximum number of allowed FW evaluations has been reached (i.e., $T_{RL} = T_{RL}^{\max}$). Otherwise, let $i \leftarrow (i+1)$ and repeat the iterative loop;

- Output the SbD -optimal PF by setting $\mathbf{A}^{SbD} = \mathbf{A}_i|_{i=I_{SbD}}$.

Since $C_{FW}^{SbD} = (T_0 + T_{RL})$ and being $T_{RL} \leq T_{RL}^{\max} \ll I$, the time saving of the SbD over the StD is given by⁽²⁾

$$\Delta t = \frac{\Delta t^{StD} - \Delta t^{SbD}}{\Delta t^{StD}} \approx \frac{(P+I) - (T_0 + T_{RL})}{(P+I)}. \quad (14)$$

Such a result indicates that the SbD is advantageous over the StD when the condition $(T_0 + T_{RL}) \ll (P+I)$ holds true.

3.1 MO - SbD as Applied to mm -Wave Automotive Radar Antenna Design

The MO - SbD method is then applied to the synthesis of mm -wave automotive radar antennas. More in detail, the MOP at hand is that of designing series-fed radiators lying on the (x, y) -plane (Fig. 5) and complying with the following (conflicting) goals: (i) a proper input impedance matching over the frequency bandwidth $[f_{\min}, f_{\max}]$, (ii) a good suppression of the sidelobes on the elevation ($\phi = 90$ [deg] - Fig. 5) plane to avoid interferences from/towards the sky (i.e., $\theta > 0$ [deg]) and the road (i.e., $\theta < 0$ [deg]), and (iii) a good beam pointing stability towards the broadside direction ($\theta_0 = 0$ [deg]) within the operative frequency band [44]. Mathematically, these requirements are coded into $Q = 3$ objectives [i.e., $\Phi_1(\underline{\Omega}) = \Phi_{S11}(\underline{\Omega})$, $\Phi_2(\underline{\Omega}) = \Phi_{SLL}(\underline{\Omega})$, and $\Phi_3(\underline{\Omega}) = \Phi_{BDD}(\underline{\Omega})$].

⁽²⁾Let us assume that in practical scenarios the time required to train, Δt_{train} , and test, Δt_{test} , the SM is negligible since $(\Delta t_{train}, \Delta t_{test}) \ll \Delta t_{FW}$ [38].

As for the resonance objective (i), let us define the following ($q = 1$)-th cost function

$$\Phi_{S_{11}}(\underline{\Omega}) \triangleq \frac{1}{B} \sum_{b=1}^B \frac{|S_{11}(f_b|\underline{\Omega})| - S_{11}^{th}}{|S_{11}^{th}|} \times \mathcal{H}\{|S_{11}(f_b|\underline{\Omega})| - S_{11}^{th}\} \quad (15)$$

where $f_b = f_{\min} + (b-1) \times \frac{(f_{\max} - f_{\min})}{(B-1)}$ is the b -th ($b = 1, \dots, B$) frequency sample ($f_b \in [f_{\min}, f_{\max}]$), S_{11} is the input reflection coefficient, S_{11}^{th} is the user-defined target threshold, and $\mathcal{H}\{\cdot\}$ is the Heaviside function ($\mathcal{H}\{\alpha\} = 1$ if $\alpha > 0$, $\mathcal{H}\{\alpha\} = 0$ otherwise).

Moreover, the two requirements on beam pattern shaping (ii) and (iii) are formulated as

$$\Phi_{SLL}(\underline{\Omega}) = \frac{1}{B} \sum_{b=1}^B \frac{SLL(f_b|\underline{\Omega}) - SLL^{th}}{|SLL^{th}|} \times \mathcal{H}\{SLL(f_b|\underline{\Omega}) - SLL^{th}\} \quad (16)$$

and

$$\Phi_{BDD}(\underline{\Omega}) = \frac{1}{B} \sum_{b=1}^B \frac{|BDD(f_b|\underline{\Omega})| - BDD^{th}}{BDD^{th}} \times \mathcal{H}\{|BDD(f_b|\underline{\Omega})| - BDD^{th}\}, \quad (17)$$

respectively. In (16), SLL and SLL^{th} are the simulated and the target sidelobe levels, while the beam direction deviation (BDD) cost term (17) is a function of the pointing direction, $BDD(f_b|\underline{\Omega}) \triangleq \arg\{\max_{\theta} \mathcal{P}(\theta, \phi = 90)\}$, $\mathcal{P}(\theta, \phi)$ being the power pattern, and the maximum allowed deviation BDD^{th} .

4 Numerical Results

The aim of this Section is two-fold. On the one hand, it deals with a preliminary assessment of the *MO-SbD* method against *MOP* benchmark functions with analytically-known *PFs* (Sect. 4.1) to also discuss the sensitivity of the optimization performance on its key calibration parameters by providing useful guidelines for the optimal setup. On the other hand, the scope of this section is that of assessing the suitability of such a *SbD* implementation to a real and challenging *MO* synthesis task. Towards this end, the design of automotive radar antennas operating in the 77 GHz band [44] has been chosen (Sect. 4.2) as a representative test case.

4.1 Assessment against *MOP* Benchmark Functions

In order to give the interested reader some insights on the *MO-SbD* working, effectiveness, and computational efficiency, as well as to assess its dependence on the control parameters, a set of numerical experiments, drawn from an extensive validation carried out on *MOP* benchmark functions, is presented hereinafter.

The first test case is concerned with the optimization of the *DTLZ1* function with $K = 3$ *DoFs* and $Q = 2$ objectives [54]. The control parameters of both the *StD/SbD* methods have been set according to the literature guidelines [46][53] as follows: $I = 1.5 \times 10^4$, $P = 15$, $W = 40$, $\gamma = 2 \times 10^{-2}$, and $\varepsilon_q = 2 \times 10^{-2}$ ($q = 1, \dots, Q$). To provide a quantitative measure of the “quality” of a *PF* \mathbf{A} , the error index, defined in [46] as

$$\xi(\mathbf{A}) = \frac{1}{A} \sum_{a=1}^A \min_{a' \in \{1, \dots, A^{act}\}} \left\| \underline{\Phi}(\underline{\Omega}^{(a)}) - \underline{\Phi}(\underline{\Omega}^{(a')}) \right\|_2 \quad (18)$$

where $\|\cdot\|$ is the ℓ_2 -norm and $\mathbf{A}^{act} = \left\{ \underline{\Omega}^{(a')}; a' = 1, \dots, A^{act} \gg A \right\}$ is the actual (analytically-computed and densely sampled) *PF*, has been evaluated.

The first analysis investigates on the dependence of the optimization performance on the number of *FW* calls ⁽³⁾ for training and updating the *SM* while evolving the *PF* towards \mathbf{A}^{SbD} . Accordingly, the sensitivity analysis has considered a variation of the number of initial training samples, T_0 , and of the maximum number of allowed *RL* calls, T_{RL}^{\max} (Sect. 3). It turns out that the setup $T_0 = (10 \times K)$ (i.e., $T_0 = 30$) and $T_{RL}^{\max} = (0.2 \times I)$ (i.e., $T_{RL}^{\max} = 3.0 \times 10^3$) is a suitable compromise between a faithful approximation of the *PF* (i.e., $\xi(\mathbf{A}^{SbD}) \Big|_{T_0/K=10}^{T_{RL}^{\max}/I=0.2} \approx 10^{-2}$) and a significant time saving with respect to the *StD* method (i.e., $\Delta t \Big|_{T_0/K=10}^{T_{RL}^{\max}/I=0.2} \approx 80\%$). For completeness, the behavior of $\xi(\mathbf{A}^{SbD})$ and Δt versus $\frac{T_0}{K}$ and $\frac{T_{RL}^{\max}}{I}$ is shown in Fig. 6(a) ($T_{RL}^{\max}/I = 0.2$) and Fig. 6(b) ($T_0/K = 10$), respectively. As expected, an increase of T_0 and/or T_{RL}^{\max} yields a better approximation of the *PF*, the values of $\xi(\mathbf{A}^{SbD})$ being smaller because of the higher accuracy of the *SM* predictions thanks to the larger set of *I/O* training samples. However, the “price to pay” is that a greater number of *FW* calls implies a lower time saving (Fig. 6). To have a more immediate understanding of the positive effects in choosing the

⁽³⁾Dealing with the benchmark functions, a *FW* call means an exact computation of the objectives associated to a guess solution.

selected (T_0, T_{RL}^{\max}) -setup, Figure 7(a) shows that the *SbD* converges to a *PF*, \mathbf{A}^{SbD} , that carefully approximates the actual one, \mathbf{A}^{act} , and it is very close to that found by the *StD* method, \mathbf{A}^{StD} [$\xi(\mathbf{A}^{StD}) = 4.2 \times 10^{-4}$ - Fig. 7(a)]. Interestingly, the solutions of the initial training set, \mathbf{T}_0 , as well as those of the initial *PF*, \mathbf{A}_0^{SbD} , are both very far from the optimal *PF* [i.e., $\xi(\mathbf{A}_0^{SbD}) = 3.1 \times 10^1$ - Fig. 7(a)]. This points out that there has been a remarkable evolution of the *PF* throughout the iterations. At the same time, it is evident the key-role of the *RL* strategy for updating the *SM* at each *FW* evaluation carried out during the *MOP* solution. As a matter of fact, the *PF* that would be determined by the *SbD*-based method without adaptively enhancing the accuracy of the *SM* is very poor as established by the corresponding error value [i.e., $\xi(\mathbf{A}^{SbD})|_{w/oRL} = 2.9 \times 10^1$ - Fig. 7(a)]. As for the number of *FW* calls during the optimization, Figure 7(b) gives the representative points in the plane $\{\Phi_1(\underline{\Omega}), \Phi_2(\underline{\Omega})\}$ of all *FW*-evaluated trial solutions by both the *SbD* and the *StD* methods. As it can be inferred, the *SbD* enables a significant reduction of the computational cost, the total number of evaluations being $C_{FW}^{SbD} = 3015$ versus $C_{FW}^{StD} = 15015$.

Similar outcomes arise when increasing the complexity of the *MOP* at hand, as well. For instance, the ability of the *SbD* to converge to the actual *PF* is confirmed also for a wider solution space with $K = 7$ variables, $\xi(\mathbf{A}^{SbD}) = 6.85 \times 10^{-3}$ ($\approx \xi(\mathbf{A}^{StD}) = 3.61 \times 10^{-3}$) being the value of the approximation error (Fig. 8). Moreover, since $P = 35$, $I = 2.0 \times 10^4$ [46], $T_0 = 70$, $T_{RL} = 3584$ ($T_{RL}^{\max} = 4 \times 10^3$), the time saving amounts to $\Delta t \simeq 82\%$.

The last test case of this Section refers to an even more challenging scenario with $Q = 3$ objectives. Once again, there is a good agreement between \mathbf{A}^{SbD} and \mathbf{A}^{act} (Fig. 9) (i.e., $\xi(\mathbf{A}^{SbD}) = 5.86 \times 10^{-3}$ close to $\xi(\mathbf{A}^{StD}) = 5.53 \times 10^{-3}$) and the time saving is kept close to $\Delta t \simeq 80\%$.

4.2 Assessment in Designing 77 GHz Automotive Radar Antennas

The suitability of the proposed *SbD* method to deal with high-dimension *MOPs* as well as the robustness of the setup of its control parameters derived in Sect. 4.1 are then assessed by addressing the computationally-expensive design of automotive radar antennas operating in the 77 [GHz] band.

The first numerical experiment is concerned with the synthesis of a slotted substrate integrated waveguide (*SIW*) antenna, whose parametric model is sketched in Fig. 10. Such a radiating structure has been modeled and simulated ($\Delta t_{FW} = 580$ [sec]) with the Ansys HFSS *FW* solver [55] by considering a Rogers RT/duroid 6002 substrate (relative permittivity $\epsilon_r = 2.94$ and loss tangent $\tan \delta = 0.0012$) of thickness $h_s = 1.27 \times 10^{-1}$ [mm]. It comprises $N = 6$ slots etched over a metallic copper film of thickness $h_c = 35$ [μm] and roughness $\rho_c = 1$ [μm]. The width w_1 of the input section of the tapered microstrip line, which is used to feed the *SIW*, has been chosen to yield a characteristic impedance of $Z_{in} = 50$ [Ω]. Moreover, the diameter of the vias, their spacing, and the width of the *SIW* have been set by following the guidelines in the state-of-the-art literature to excite the dominant mode TE_{10} (i.e., $d_{via} = 2.03 \times 10^{-1}$ [mm], $s_{via} = 4.06 \times 10^{-1}$ [mm], and $w_{SIW} = 1.85$ [mm] - Fig. 10) [56].

The arising *MOP* has been defined with the $Q = 3$ objectives detailed in Sect. 3.1 by assuming $f_{\min} = 76$ [GHz], $f_{\max} = 79$ [GHz], $B = 7$, $S_{11}^{th} = -15$ [dB], $SLL^{th} = -20$ [dB], and $BDD^{th} = 0.25$ [deg]. As for the dimension of the solution space, $K = 10$ geometrical descriptors, $\underline{\Omega} = \{\Omega_k; k = 1, \dots, K\}$, have been optimized (Fig. 10) by considering the following assignment: $(\Omega_1, \Omega_2) = (l_1, w_2)$, l_1 and w_2 being the *DoFs* that control the *SIW* input section; $(\Omega_3, \Omega_4) = (s_{y,1}, s_{y,2})$, $s_{y,1}$ and $s_{y,2}$ being the initial and the final offsets; $(\Omega_5, \Omega_6, \Omega_7) = (s_s, s_l, s_w)$, s_s , s_l , and s_w being the spacing, the length, and the width of the slot, respectively; $(\Omega_8, \Omega_9, \Omega_{10}) = (s_{x,1}, s_{x,2}, s_{x,3})$, $s_{x,1}$, $s_{x,2}$, and $s_{x,3}$ being the offset from the longitudinal axis of the first $\frac{N}{2}$ slots (i.e., $n = 1, \dots, \frac{N}{2}$), while the other ones (i.e., $n = (\frac{N}{2} + 1), \dots, N$) are yielded with a mirroring operation to keep the geometric/electric symmetry of the structure.

Figure 11(a) shows the *SbD*-optimized solutions belonging to the final ($i = I$) *PF* \mathbf{A}^{SbD} [$P = 50$, $T_0 = 100$, $T_{RL} = 2.05 \times 10^3$ ($T_{RL}^{\max} = 4.0 \times 10^3$)] that comprises $A^{SbD} = 8$ trade-off *SIW* designs. The *PF* solutions that globally minimize each objective [i.e., $\underline{\Omega}_q^{SbD}$ ($q = 1, \dots, Q$) being $\underline{\Omega}_q^{SbD} = \arg \{ \min_{\underline{\Omega} \in \mathbf{A}^{SbD}} \Phi_q(\underline{\Omega}) \}$] are reported, as well. For comparison purposes, the same plot for the *StD* is shown in Fig. 11(b), as well.

Figure 12 details the performance of $\underline{\Omega}_q^{SbD}$ ($q = 1, \dots, Q$) in terms of bandwidth [Fig. 12(a)], *SLL* [Fig. 12(b)], and *BDD* [Fig. 12(c)]. As expected, the solution $\underline{\Omega}_{S_{11}}^{SbD}$ is the unique so-

lution fully compliant with the S_{11} requirement since $|S_{11}(f|\underline{\Omega}_{S_{11}}^{SbD})|_{dB} \leq S_{11}^{th}$ whatever $f \in [f_{\min}, f_{\max}]$ [Fig. 12(a)], but it corresponds to a sub-optimal SLL [i.e., $SLL(f|\underline{\Omega}_{S_{11}}^{SbD}) \leq -18.9$ [dB] - Fig. 12(b)] and BDD [i.e., $|BDD(f|\underline{\Omega}_{S_{11}}^{SbD})| \leq 1$ [deg] - Fig. 12(c)] performance. The other two trade-off solutions present a similar, but complementary, behavior (Fig. 12). For illustrative purposes, Figure 13 plots the normalized power pattern along the $\phi = 90$ cut at the central frequency (i.e., $f = 77.5$ [GHz]). It turns out that the best SLL value is $SLL(f|\underline{\Omega}_{SLL}^{SbD}) \leq -21.8$ [dB] [Fig. 12(b)], while the beam pointing is very stable in the whole working band when $\underline{\Omega} = \underline{\Omega}_{BDD}^{SbD}$ [i.e., $BDD(f|\underline{\Omega}_{BDD}^{SbD}) = 0$ [deg] - Fig. 12(c)].

By comparing the SbD -optimized PF with that found by the StD method [Fig. 11(a) vs. Fig. 11(b)], it turns out that the interpolation surfaces look very similar as well as the distribution of the representative points, while the computational costs for determining those solutions are very different, the time saving being equal to $\Delta t \simeq 89\%$ when using the MO - SbD instead of the StD method. Let us now consider the best trade-off solution, according to the ‘‘Minimum Manhattan Distance’’ (MMD) criterion [10] ($\underline{\Omega}^*$ - see Appendix II), found by the two methods (i.e., $\underline{\Omega}^{SbD}$ [Fig. 11(a)] and $\underline{\Omega}^{StD}$ [Fig. 11(b)]). The frequency behavior of the S_{11} [Fig. 14(a)], the SLL [Fig. 14(b)], and the BDD [Fig. 14(c)] of these solutions is reported in Figure 14, while the corresponding central frequency patterns are shown in Fig. 15(a). As it can be observed, the two solutions exhibit almost identical performance thanks to the similarity of the antenna layouts [Fig. 15(b) vs. Fig. 15(c)] also confirmed by the values of their geometric descriptors (Tab. III).

To further assess the potentialities of the MO - SbD method in designing automotive radar antennas, the second experiment deals with the synthesis of a perturbed travelling-wave open stubs ($PTOS$) comb-line array composed by $N = 7$ series-fed radiating elements [Fig. 16(a)] [57]. The guideline of the design is that of considering a different width for each microstrip line connecting the stubs [i.e., $l_{w,1} \neq l_{w,2} \neq l_{w,3} \neq l_{w,4}$ - Fig. 16(a)] so that a better impedance matching can be achieved along different sections of the antenna layout, which is terminated on a matched load ($Z_L = 50$ [Ω]). Moreover, the stubs are allowed to have different widths [i.e., $o_{w,1} \neq o_{w,2} \neq o_{w,3} \neq o_{w,4}$ - Fig. 16(a)] to let them implement the desired current tapering to

lower the *SLL* of a uniform structure [57]⁽⁴⁾. Accordingly, the antenna layout has been parameterized with $K = 11$ *DoFs*, $\underline{\Omega} = \{l_{l,1}, l_{l,2}, l_{w,1}, l_{w,2}, l_{w,3}, l_{w,4}, o_{w,1}, o_{w,2}, o_{w,3}, o_{w,4}, o_l\}$ [Fig. 16(a)].

Figure 16(b) shows the *SbD*-synthesized *PF* solutions, while Figure 17 compares the performance indexes of $\underline{\Omega}_{S_{11}}^{SbD}$, $\underline{\Omega}_{SLL}^{SbD}$, $\underline{\Omega}_{BDD}^{SbD}$, and $\underline{\Omega}^{SbD}$ versus the frequency, $f \in [f_{\min}, f_{\max}]$. Generally speaking, the results confirm the effectiveness of the *SbD* method in efficiently (i.e., $\Delta t \simeq 89\%$) synthesizing antenna designs that fulfil contrasting requirements so that the designer can select the most suitable layout for different specific applications. The higher (with respect to the *SIW*), but yet acceptable beam squint [i.e., $|BDD(f)| \leq 2$ [deg] - Fig. 17(c)], is expected and mainly due to the travelling-wave structure [58] at hand.

For completeness, representative radiation patterns at $f = 77.5$ [GHz] are shown in Fig. 18(a), while the *HFSS* screen-shot and the *DoFs* of the optimal trade-off solution synthesized with the *SbD* are reported in Fig. 18(b) and Tab. IV, respectively.

5 Conclusions and Final Remarks

A new computationally-efficient method for the *MO* design of complex *EM* devices has been proposed by leveraging on an effective integration of evolutionary optimization strategies and *AI* concepts. The arising *MO-SbD* method allows one an effective sampling of the solution space to provide the decision maker a set of optimal trade-off solutions that fit conflicting requirements (e.g., impedance matching and far-field radiation features in antenna design).

The numerical validation, concerned with benchmark *MOPs* as well as real antennas for automotive radars, has outputted the following main outcomes:

- the *MO-SbD* method performs an effective sampling of high-dimensional solution spaces being able to retrieve a *PF* of compromise solutions close to that found by the *StD* approach and to the analytically-computed one in the case of benchmark functions;
- the huge time saving ($\Delta t \geq 80\%$) of the *MO-SbD* is achieved thanks to the exploitation of

⁽⁴⁾Analogously to the *SIW* design, the second half of open stubs (i.e., $n = (\lceil \frac{N}{2} \rceil + 1), \dots, N$) are obtained from the first $\lceil \frac{N}{2} \rceil$ ones by means of a mirroring operation to enforce a better sidelobes symmetry around the broadside [Fig. 16(a)].

AI-based mechanisms (i.e., *SM* and *RL*), while the *StD* approach is highly computationally-demanding since it is exclusively based on *FW* evaluations;

- the *MO-SbD* method proved to be a reliable, effective, and computationally efficient tool for the *MO* design of *mm*-wave automotive radar antennas working in the 77 [GHz] band either based on *SIW* or *PTOS* architectures.

Future works, beyond the scope of this paper, will be aimed at exploiting (i) properly customized deep learning architectures to enable an unprecedented prediction accuracy [29] as well as (ii) adaptive and/or Compressive sampling strategies [18] to generate highly-informative and low-cardinality training sets. Finally, the prototyping of the synthesized *mm*-wave automotive radiators as well as their experimental validation, besides the *FW* numerical assessment with *HFSS* in this paper, are under investigation by some industrial partners.

Acknowledgements

This work has been partially supported by the Italian Ministry of Education, University, and Research within the PRIN 2017 Program, for the Project “Cloaking Metasurfaces for a New Generation of Intelligent Antenna Systems (MANTLES)” (Grant No. 2017BHFZKH - CUP: E64I19000560001) and the Project "CYBER-PHYSICAL ELECTROMAGNETIC VISION: Context-Aware Electromagnetic Sensing and Smart Reaction (EMvisioning)" (Grant no. 2017HZJXSZ - CUP: E64I19002530001), within the Program "Progetti di Ricerca Industriale e Sviluppo Sperimentale nelle 12 aree di specializzazione individuate dal PNR 2015-2020", Specialization Area "Smart Secure & Inclusive Communities" for the Project "Mitigazione dei rischi naturali per la sicurezza e la mobilita' nelle aree montane del Mezzogiorno (MITIGO)" (Grant no. ARS01_00964), and within the Program "Smart cities and communities and Social Innovation" for the Project "Piattaforma Intelligente per il Turismo (SMARTOUR)" (Grant no. SCN_00166 - CUP: E44G14000040008). Moreover, it benefited from the networking activities carried out within the Project “SPEED” (Grant No. 61721001) funded by National Science Foundation of China under the Chang-Jiang Visiting Professorship Program. A. Massa wishes to thank E. Vico for her never-ending inspiration, support, guidance, and help.

Appendix I

In (13), the maximum crowding distance $\Gamma(\mathbf{A}_{i-w})$ is defined as [53]

$$\Gamma(\mathbf{A}_{i-w}) = \max_{a=2, \dots, (A_{i-w}-1)} \left\{ \sum_{q=1}^Q D_q(\underline{\Omega}_{i-w}^{(a)}) \right\} \quad (19)$$

where the q -th ($q = 1, \dots, Q$) distance is computed as

$$D_q(\underline{\Omega}_{i-w}^{(a)}) = \Phi_q(\underline{\Omega}_{i-w}^{(a+1)}) - \Phi_q(\underline{\Omega}_{i-w}^{(a-1)}) \quad (20)$$

by setting

$$\begin{aligned} \underline{\Omega}_{i-w}^{(a)} \Big|_{a=1} &= \arg \left\{ \min_{v=1, \dots, A} \left[\Phi_q(\underline{\Omega}_{i-w}^{(v)}) \right] \right\} \\ \underline{\Omega}_{i-w}^{(a)} \Big|_{a=A_{i-w}} &= \arg \left\{ \max_{v=1, \dots, A} \left[\Phi_q(\underline{\Omega}_{i-w}^{(v)}) \right] \right\} \end{aligned} \quad (21)$$

and ordering the remaining [$a = 2, \dots, (A_{i-w} - 1)$] *PF* elements so that

$$\Phi_q(\underline{\Omega}_{i-w}^{(a-1)}) \leq \Phi_q(\underline{\Omega}_{i-w}^{(a)}) \leq \Phi_q(\underline{\Omega}_{i-w}^{(a+1)}). \quad (22)$$

Moreover, the average crowding distance over a window of W iterations is defined as [53]

$$\bar{\Gamma}_i = \frac{1}{W} \sum_{w=0}^{W-1} \Gamma(\mathbf{A}_{i-w}). \quad (23)$$

Appendix II

According to the *MMD* criterion, the best trade-off solution, $\underline{\Omega}^*$, is given by [10]

$$\underline{\Omega}^* = \arg \left\{ \min_{a=1, \dots, A} \left\| \underline{\Phi}'(\underline{\Omega}^{(a)}) - \underline{\Phi}^{ideal} \right\|_1 \right\} \quad (24)$$

where $\|\cdot\|_1$ is the ℓ_1 -norm, while the q -th ($q = 1, \dots, Q$) entry of $\underline{\Phi}'(\underline{\Omega}^{(a)}) = \{\Phi'_q(\underline{\Omega}^{(a)}); q = 1, \dots, Q\}$ and $\underline{\Phi}^{ideal} = \{\Phi_q^{ideal}; q = 1, \dots, Q\}$ is given by

$$\Phi'_q(\underline{\Omega}^{(a)}) = \frac{\Phi_q(\underline{\Omega}^{(a)})}{\max_{a=1, \dots, A} \left\{ \Phi_q(\underline{\Omega}^{(a)}) \right\} - \min_{a=1, \dots, A} \left\{ \Phi_q(\underline{\Omega}^{(a)}) \right\}} \quad (25)$$

and

$$\Phi_q^{ideal} = \min_{a=1,\dots,A} \left\{ \Phi'_q \left(\underline{\Omega}^{(a)} \right) \right\}, \quad (26)$$

respectively.

References

- [1] W. Zhang, F. Feng, W. Liu, S. Yan, J. Zhang, J. Jin, and Q.-J. Zhang "Advanced parallel space-mapping-based multiphysics optimization for high-power microwave filters," *IEEE Trans. Microw. Theory Techn.*, vol. 69, no. 5, pp. 2470-2484, May 2021.
- [2] L. Wang, G. Wang and J. Siden, "Design of high-directivity wideband microstrip directional coupler with fragment-type structure," *IEEE Trans. Microw. Theory Techn.*, vol. 63, no. 12, pp. 3962-3970, Dec. 2015.
- [3] A. O. Watanabe, T.-H. Lin, M. Ali, Y. Wang, V. Smet, P. M. Raj, M. M. Tentzeris, R. R. Tummala, and M. Swaminathan, "Ultrathin antenna-integrated glass-based millimeter-wave package with through-glass vias," *IEEE Trans. Microw. Theory Techn.*, vol. 68, no. 12, pp. 5082-5092, Dec. 2020.
- [4] S. Goudos, *Emerging Evolutionary Algorithms for Antennas and Wireless Communications*. Stevenage: SciTech Publishing Inc., 2021.
- [5] S. Amari, "Synthesis of cross-coupled resonator filters using an analytical gradient-based optimization technique," *IEEE Trans. Microw. Theory Techn.*, vol. 48, no. 9, pp. 1559-1564, Sep. 2000.
- [6] P. Rocca, M. Benedetti, M. Donelli, D. Franceschini, and A. Massa, "Evolutionary optimization as applied to inverse scattering problems," *Inverse Problems*, vol. 24, no. 12, pp. 1-41, 2009.
- [7] S. K. Goudos, K. Siakavara, T. Samaras, E. E. Vafiadis, and J. N. Sahalos, "Self-adaptive differential evolution applied to real-valued antenna and microwave design problems," *IEEE Trans. Antennas Propag.*, vol. 59, no. 4, pp. 1286-1298, Apr. 2011.

- [8] S. K. Goudos, C. Kalialakis, and R. Mittra, "Evolutionary algorithms applied to antennas and propagation: A review of state of the art," *Int. J. Antennas Propag.*, vol. 2016, pp. 1-12, Jan. 2016.
- [9] J. Nagar and D. H. Werner, "A comparison of three uniquely different state of the art and two classical multiobjective optimization algorithms as applied to electromagnetics," *IEEE Trans. Antennas Propag.*, vol. 65, no. 3, pp. 1267-1280, Mar. 2017.
- [10] P. Rocca, N. Anselmi, A. Polo, and A. Massa, "Pareto-optimal domino-tiling of orthogonal polygon phased arrays," *IEEE Trans. Antennas Propag.*, 2022 to be published.
- [11] M. Matalatala, M. Deruyck, S. Shikhantsov, E. Tanghe, D. Plets, S. Goudos, K. El. Psnanis, L. Martens, and W. Joseph, "Multi-objective optimization of massive MIMO 5G wireless networks towards power consumption, uplink and downlink exposure," *Appl. Sci.*, vol. 9, pp. 1-20, 2019.
- [12] J. Nagar, S. D. Campbell, Q. Ren, J. A. Easum, R. P. Jenkins, and D. H. Werner, "Multi-objective optimization-aided metamaterials-by-design with application to highly directive nanodevices," *IEEE J. Multiscale Multiphys. Comput. Tech.*, vol. 2, pp. 147-158, 2017.
- [13] R. F. Harrington, *Field Computational by Moment Methods*. Hoboken, NJ, USA: Wiley, 1993.
- [14] D. Davidson, *Computational Electromagnetic for RF Microwave Engineering*. Cambridge, U.K.: Cambridge Univ. Press, 2011.
- [15] Z. Chen, C.-F. Wang and W. J. R. Hoefer, "A unified view of computational electromagnetics," *IEEE Trans. Microw. Theory Techn.*, vol. 70, no. 2, pp. 955-969, Feb. 2022.
- [16] C. Balanis, *Antenna theory: analysis and design*. Hoboken, N.J.: Wiley, 2016.
- [17] D. R. Jackson and N. G. Alexopoulos, "Simple approximate formulas for input resistance, bandwidth, and efficiency of a resonant rectangular patch," *IEEE Trans. Antennas Propag.*, vol. 39, no. 3, pp. 407-410, Mar. 1991.

- [18] A. Massa, P. Rocca, and G. Oliveri, "Compressive sensing in electromagnetics - A review," *IEEE Antennas Propag. Mag.*, pp. 224-238, vol. 57, no. 1, Feb. 2015.
- [19] M. Salucci, G. Oliveri, M. A. Hannan, and A. Massa, "System-by-Design paradigm-based synthesis of complex systems: The case of spline-contoured 3D radomes," *IEEE Antennas Propag. Mag.*, vol. 64, no. 1, pp. 72-83, Feb. 2022.
- [20] G. Oliveri and A. Massa, "GA-enhanced ADS-based approach for array thinning," *IET Microw., Antennas Propag.*, vol. 5, no. 3, pp. 305-315, 2011.
- [21] S. Koziel, J. W. Bandler and Q. S. Cheng, "Robust trust-region space-mapping algorithms for microwave design optimization," *IEEE Trans. Microw. Theory Techn.*, vol. 58, no. 8, pp. 2166-2174, Aug. 2010.
- [22] W. Zhang, F. Feng, V.-M.-R. Gongal-Reddy, J. Zhang, S. Yan, J. Ma, and Q.-J. Zhang, "Space mapping approach to electromagnetic centric multiphysics parametric modeling of microwave components," *IEEE Trans. Microw. Theory Techn.*, vol. 66, no. 7, pp. 3169-3185, Jul. 2018.
- [23] S. Koziel and M. Abdullah, "Machine-learning-powered EM-based framework for efficient and reliable design of low scattering metasurfaces," *IEEE Trans. Microw. Theory Techn.*, vol. 69, no. 4, pp. 2028-2041, Apr. 2021.
- [24] L. Cui, Y. Zhang, R. Zhang, and Q. Huo Liu, "A modified efficient KNN method for antenna optimization and design," *IEEE Trans. Antennas Propag.*, vol. 68, no. 10, pp. 6858-6866, Oct. 2020.
- [25] A. Toktas, D. Ustun, and M. Tekbas, "Multi-objective design of multi-layer radar absorber using surrogate-based optimization," *IEEE Trans. Microw. Theory Techn.*, vol. 67, no. 8, pp. 3318-3329, Aug. 2019.
- [26] S. Koziel and A. Pietrenko-Dabrowska, "Fast multi-objective optimization of antenna structures by means of data-driven surrogates and dimensionality reduction," *IEEE Access*, vol. 8, pp. 183300-183311, Oct. 2020.

- [27] J. Long, Y. Liao, and P. Yu, "Multi-response weighted adaptive sampling approach based on hybrid surrogate model," *IEEE Access*, vol. 9, pp. 45441-45453, Mar. 2021.
- [28] A. Massa, G. Oliveri, M. Salucci, N. Anselmi, and P. Rocca, "Learning-by-examples techniques as applied to electromagnetics," *J. Electromagn. Waves Appl.*, vol. 32, no. 4, pp. 516-541, 2018.
- [29] A. Massa, D. Marcantonio, X. Chen, M. Li, and M. Salucci, "DNNs as applied to electromagnetics, antennas, and propagation - A review," *IEEE Antennas Wireless Propag. Lett.* vol. 18, no. 11, pp. 2225-2229, Nov. 2019.
- [30] Q. Wu, W. Chen, C. Yu, H. Wang, and W. Hong, "Multilayer machine learning-assisted optimization-based robust design and its applications to antennas and array," *IEEE Trans. Antennas Propag.*, vol. 69, no. 9, pp. 6052-6057, Sep. 2021.
- [31] J. Nan, H. Xie, M. Gao, Y. Song, and W. Yang, "Design of UWB antenna based on improved deep belief network and extreme learning machine surrogate models," *IEEE Access*, vol. 9, pp. 126541-126549, 2021.
- [32] C. Lewis, J. Bryan, N. Schwartz, J. Hale, K. Fanning and J. S. Colton, "Machine learning to predict quasi TE_{00} mode resonances in double-stacked dielectric cavities," *IEEE Trans. Microw. Theory Techn.*, to be published.
- [33] J. A. Easum, J. Nagar, P. L. Werner, and D. H. Werner, "Efficient multiobjective antenna optimization with tolerance analysis through the use of surrogate models," *IEEE Trans. Antennas Propag.*, vol. 66, no. 12, pp. 6706-6715, Dec. 2018.
- [34] J. Dong, W. Qin, and M. Wang, "Fast multi-objective optimization of multi-parameter antenna structures based on improved BPNN surrogate model," *IEEE Access*, vol. 7, pp. 77692-77701, 2019.
- [35] B. Liu, M. O. Akinsolu, C. Song, Q. Hua, P. Excell, Q. Xu, Y. Huang, and M. Ali Imran, "An efficient method for complex antenna design based on a self adaptive surrogate model-assisted optimization technique," *IEEE Trans. Antennas Propag.*, vol. 69, no. 4, pp. 2302-2315, Apr. 2021.

- [36] Y. Ma, Y. Xiao, J. Wang, and L. Zhou, "Multicriteria optimal Latin hypercube design-based surrogate-assisted design optimization for a permanent-magnet vernier machine," *IEEE Trans. Magn.*, vol. 58, no. 2, pp. 1-5, Feb. 2022.
- [37] S. An, S. Yang, and O. A. Mohammed, "A kriging-assisted light beam search method for multi-objective electromagnetic inverse problems," *IEEE Trans. Magn.*, vol. 54, no. 3, pp. 1-4, Mar. 2018.
- [38] A. Massa and M. Salucci, "On the design of complex EM devices and systems through the System-by-Design paradigm - A framework for dealing with the computational complexity," *IEEE Trans. Antennas Propag.*, vol. 70, no. 2, pp. 1328-1343, Feb. 2022.
- [39] G. Oliveri, M. Salucci, R. Lombardi, R. Flamini, C. Mazzucco, S. Verzura, and A. Massa, "WAIM-Enhanced dual-polarization sub-6 GHz wide-scan array for next generation base stations," *IEEE Trans. Antennas Propag.*, to be published.
- [40] M. Salucci, L. Tenuti, G. Gottardi, A. Hannan, and A. Massa, "A System-by-Design method for efficient linear array miniaturization through low-complexity isotropic lenses," *Electron. Lett.*, vol. 55, no. 8, pp. 433-434, Apr. 2019.
- [41] G. Oliveri, P. Rocca, M. Salucci, and A. Massa, "Holographic smart EM skins for advanced beam power shaping in next generation wireless environments," *IEEE J. Multiscale Multiphys. Comput. Tech.*, vol. 6, pp. 171-182, 2021.
- [42] E. Arnieri, M. Salucci, F. Greco, L. Boccia, A. Massa, and G. Amendola, "An equivalent circuit/system-by-design approach to the design of reflection-type dual-band circular polarizers," *IEEE Trans. Antennas Propag.*, to be published, doi: 10.1109/TAP.2021.3111511.
- [43] G. Oliveri, A. Gelmini, A. Polo, N. Anselmi, and A. Massa, "System-by-design multi-scale synthesis of task-oriented reflectarrays," *IEEE Trans. Antennas Propag.*, vol. 68, no. 4, pp. 2867-2882, Apr. 2020.

- [44] J. Hasch, E. Topak, R. Schnabel, T. Zwick, R. Weigel, and C. Waldschmidt, "Millimeter-Wave technology for automotive radar sensors in the 77 GHz frequency band," *IEEE Trans Microw. Theory Techn.*, vol. 60, no. 3, pp. 845-860, Mar. 2012.
- [45] K. Deb, *Multi-Objective Optimization Using Evolutionary Algorithms*. West Sussex, U.K.: Wiley, 2001.
- [46] K. Deb, M. Mohan, and B. Mishra, "A fast multi-objective evolutionary algorithm for finding well-spread Pareto-optimal solutions," *KanGAL Report*, no. 2003002, 2003.
- [47] D. R. Jones, M. Schonlau, and W. J. Welch, "Efficient global optimization of expensive black-box functions," *J. Global Optim.*, vol. 13, no. 4, pp. 455-492, Jun. 1998.
- [48] J. Sacks, W. J. Welch, T. J. Mitchell, and H. P. Wynn, "Design and analysis of computer experiments," *Statist. Sci.*, vol. 4, no. 4, pp. 409-423, 1989.
- [49] M. Salucci, L. Tenuti, G. Oliveri, and A. Massa, "Efficient prediction of the EM response of reflectarray antenna elements by an advanced statistical learning method," *IEEE Trans. Antennas Propag.*, vol. 66, no. 8, pp. 3995-4007, Aug. 2018.
- [50] M. Laumanns, L. Thiele, K. Deb, and E. Zitzler, "Combining convergence and diversity in evolutionary multiobjective optimization," *Evol. Comp.*, vol. 10, no. 3, pp. 263-282, Mar. 2002.
- [51] K. Deb and R. B. Agrawal, "Simulated binary crossover for continuous search space," *Complex Systems*, vol. 9, no. 2, pp. 115-148, Feb. 1995.
- [52] K. Deb and M. Goyal, "A combined genetic adaptive search (GeneAS) for engineering design," *Computer Sci. Informatics*, vol. 26, no. 4, pp. 30-45, Apr. 1996.
- [53] O. Roudenko and M. Schoenauer, "A steady performance stopping criterion for Pareto-based evolutionary algorithms," in *Proc. 6th Int. Multi-Objective Programming & Goal Programming Conf.*, Apr. 2004, Hammamet, Tunisia.

- [54] K. Deb, L. Thiele, M. Laumanns, and E. Zitzler, “Scalable test problems for evolutionary multi-objective optimization,” *Technical Report*, Computer Engineering and Networks Laboratory (TIK), Swiss Federal Institute of Technology (ETH), 2001.
- [55] ANSYS Electromagnetics Suite - HFSS (2021). ANSYS, Inc.
- [56] D. Deslandes and K. Wu, “Accurate modeling, wave mechanisms, and design considerations of a substrate integrated waveguide,” *IEEE Trans. Microw. Theory, Tech.*, vol. 54, no. 6, pp. 2516-2526, Jun. 2006.
- [57] L. Zhang, W. Zhang, and Y. P. Zhang, “Microstrip grid, and comb array antennas,” *IEEE Trans. Antennas Propag.*, vol. 59, no. 11, pp. 4077-4084, Nov. 2011.
- [58] S. T. Choi and Y. H. Kim, “Microstrip travelling wave combline array antenna with reflection compensation,” *Electron. Lett.*, vol. 42, no. 21, pp. 1196-1197, Oct. 2006.
- [59] P. Rocca, G. Oliveri, R. J. Mailloux, and A. Massa, “Unconventional phased array architectures and design methodologies - A review,” *Proc. IEEE*, vol. 104, no. 3, pp. 544-560, Mar. 2016.
- [60] F. Viani, F. Robol, M. Salucci, and R. Azaro, “Automatic EMI filter design through particle swarm optimization,” *IEEE Trans. Electromagnet. Compat.*, vol. 59, no. 4, pp. 1079-1094, Aug. 2017.

FIGURE CAPTIONS

- **Figure 1.** *Dominance/ ε -Dominance* ($Q = 2$) - Illustrative example with the solutions $\underline{\Omega}^{(1)}$, $\underline{\Omega}^{(2)}$, and $\underline{\Omega}^{(3)}$: $\underline{\Omega}^{(1)} \prec \underline{\Omega}^{(3)}$, $\underline{\Omega}^{(2)} \prec \underline{\Omega}^{(3)}$, $\underline{\Omega}^{(1)} \not\prec \underline{\Omega}^{(2)}$, $\underline{\Omega}^{(2)} \not\prec \underline{\Omega}^{(1)}$, $\underline{\Omega}^{(1)} \prec_{\varepsilon} \underline{\Omega}^{(2)}$, $\underline{\Omega}^{(1)} \prec_{\varepsilon} \underline{\Omega}^{(3)}$, and $\underline{\Omega}^{(2)} \prec_{\varepsilon} \underline{\Omega}^{(3)}$.
- **Figure 2.** Pictorial representation of the “confidence hyper-volume” of the prediction $\tilde{\Phi}(\underline{\Omega})$.
- **Figure 3.** *SbD-Dominance* ($Q = 2$) - Pictorial representation of $\underline{\Omega}^{(1)} \prec_{sbD} \underline{\Omega}^{(2)}$ when (a) $\tilde{\Phi}(\underline{\Omega}^{(1)})$ and $\tilde{\Phi}(\underline{\Omega}^{(2)})$, (b) $\Phi(\underline{\Omega}^{(1)})$ and $\Phi(\underline{\Omega}^{(2)})$, (c) $\tilde{\Phi}(\underline{\Omega}^{(1)})$ and $\Phi(\underline{\Omega}^{(2)})$, (d) $\Phi(\underline{\Omega}^{(1)})$ and $\Phi(\underline{\Omega}^{(2)})$.
- **Figure 4.** *MO-SbD Method* - Block diagram.
- **Figure 5.** Sketch of the automotive radar scenario.
- **Figure 6.** *Sensitivity Analysis (DTLZI Benchmark Function, $K = 3, Q = 2$ [54], $I = 1.5 \times 10^4, P = 15$)* - Behavior of the time saving, Δt , and of the *PF* approximation error, $\xi(\mathbf{A}^{SbD})$, versus (a) $\frac{T_0}{K}$ ($\frac{T_{RL}^{\max}}{I} = 0.2$) and (b) $\frac{T_{RL}^{\max}}{I}$ ($\frac{T_0}{K} = 10$).
- **Figure 7.** *Sensitivity Analysis (DTLZI Benchmark Function, $K = 3, Q = 2$ [54], $I = 1.5 \times 10^4, P = 15, T_0 = 30, T_{RL}^{\max} = 3.0 \times 10^3$)* - Representative points in the (Φ_1, Φ_2) -plane of the *MOP* solutions.
- **Figure 8.** *Sensitivity Analysis (DTLZI Benchmark Function, $K = 7, Q = 2$ [54], $I = 2.0 \times 10^4, P = 35, T_0 = 70, T_{RL}^{\max} = 4.0 \times 10^3$)* - Representative points in the (Φ_1, Φ_2) -plane of the *MOP* solutions.
- **Figure 9.** *Sensitivity Analysis (DTLZI Benchmark Function, $K = 7, Q = 3$ [54], $I = 2.0 \times 10^4, P = 35, T_0 = 70, T_{RL}^{\max} = 4.0 \times 10^3$)* - Representative points in the (Φ_1, Φ_2, Φ_3) -space of the *MOP* solutions.
- **Figure 10.** *Automotive Radar Antenna Design (SIW Radiator, $K = 10, Q = 3$)* - Sketch of the geometry of the antenna model along with the *DoF*s of the antenna synthesis problem.

- **Figure 11.** *Automotive Radar Antenna Design (SIW Radiator, $K = 10, Q = 3, I = 2.0 \times 10^4, P = 50, T_0 = 100, T_{RL}^{\max} = 4.0 \times 10^3$)* - Representative points in the (Φ_1, Φ_2, Φ_3) -space of (a) the *SbD* and (b) the *StD* PFs solutions.
- **Figure 12.** *Automotive Radar Antenna Design (SIW Radiator, $K = 10, Q = 3, I = 2.0 \times 10^4, P = 50, T_0 = 100, T_{RL}^{\max} = 4.0 \times 10^3$)* - Behavior of (a) the S_{11} , (b) the *SLL*, and (c) the *BDD* versus the frequency of *MOP* solutions $\underline{\Omega}_{S_{11}}^{SbD}$, $\underline{\Omega}_{SLL}^{SbD}$, and $\underline{\Omega}_{BDD}^{SbD}$.
- **Figure 13.** *Automotive Radar Antenna Design (SIW Radiator, $K = 10, Q = 3, I = 2.0 \times 10^4, P = 50, T_0 = 100, T_{RL}^{\max} = 4.0 \times 10^3$)* - Normalized elevation pattern, $\mathcal{P}(\theta, \phi = 90)$, radiated at $f = 77.5$ [GHz] by the *MOP* solutions $\underline{\Omega}_{S_{11}}^{SbD}$, $\underline{\Omega}_{SLL}^{SbD}$, and $\underline{\Omega}_{BDD}^{SbD}$.
- **Figure 14.** *Automotive Radar Antenna Design (SIW Radiator, $K = 10, Q = 3, I = 2.0 \times 10^4, P = 50, T_0 = 100, T_{RL}^{\max} = 4.0 \times 10^3$)* - Behavior of the (a) S_{11} , (b) *SLL*, and (c) *BDD* versus frequency for the compromise solutions found by the *SbD*, $\underline{\Omega}^{SbD}$, and the *StD*, $\underline{\Omega}^{StD}$, methods.
- **Figure 15.** *Automotive Radar Antenna Design (SIW Radiator, $K = 10, Q = 3, I = 2.0 \times 10^4, P = 50, T_0 = 100, T_{RL}^{\max} = 4.0 \times 10^3$)* - Normalized elevation pattern, $\mathcal{P}(\theta, \phi = 90)$, radiated at $f = 77.5$ [GHz] by (b) the *SbD* and (c) the *StD* antenna layouts.
- **Figure 16.** *Automotive Radar Antenna Design (PTOS Radiator, $K = 11, Q = 3, I = 2.0 \times 10^4, P = 55, T_0 = 110, T_{RL}^{\max} = 4.0 \times 10^3$)* - (a) Sketch of the geometry of the antenna model along with the *DoFs* of the antenna synthesis problem and (b) representative points in the (Φ_1, Φ_2, Φ_3) -space of the *SbD* PF solutions.
- **Figure 17.** *Automotive Radar Antenna Design (PTOS Radiator, $K = 11, Q = 3, I = 2.0 \times 10^4, P = 55, T_0 = 110, T_{RL}^{\max} = 4.0 \times 10^3$)* - Behavior of (a) the S_{11} , (b) the *SLL*, and (c) the *BDD* versus the frequency of *MO-SbD* representative solutions.
- **Figure 18.** *Automotive Radar Antenna Design (PTOS Radiator, $K = 11, Q = 3, I = 2.0 \times 10^4, P = 55, T_0 = 110, T_{RL}^{\max} = 4.0 \times 10^3$)* - (a) Normalized elevation pattern, $\mathcal{P}(\theta, \phi = 90)$, radiated at $f = 77.5$ [GHz] by the *MO-SbD* representative solutions and (b) layout of the *SbD* antenna.

TABLE CAPTIONS

- **Table I.** *SbD-Dominance* ($Q = 2$) - Rules for the condition $\underline{\Omega}^{(1)} \prec_{sbD} \underline{\Omega}^{(2)}$.
- **Table II.** *MO-SbD* - Rules for the population update ($\mathbf{P}_{i-1} \rightarrow \mathbf{P}_i$) at the i -th ($i = 1, \dots, I$) iteration.
- **Table III.** *Automotive Radar Antenna Design (SIW Radiator, $K = 10, Q = 3, I = 2.0 \times 10^4, P = 50, T_0 = 100, T_{RL}^{\max} = 4.0 \times 10^3$) - DoFs values.*
- **Table IV.** *Automotive Radar Antenna Design (PTOS Radiator, $K = 11, Q = 3, I = 2.0 \times 10^4, P = 55, T_0 = 110, T_{RL}^{\max} = 4.0 \times 10^3$) - DoFs values.*

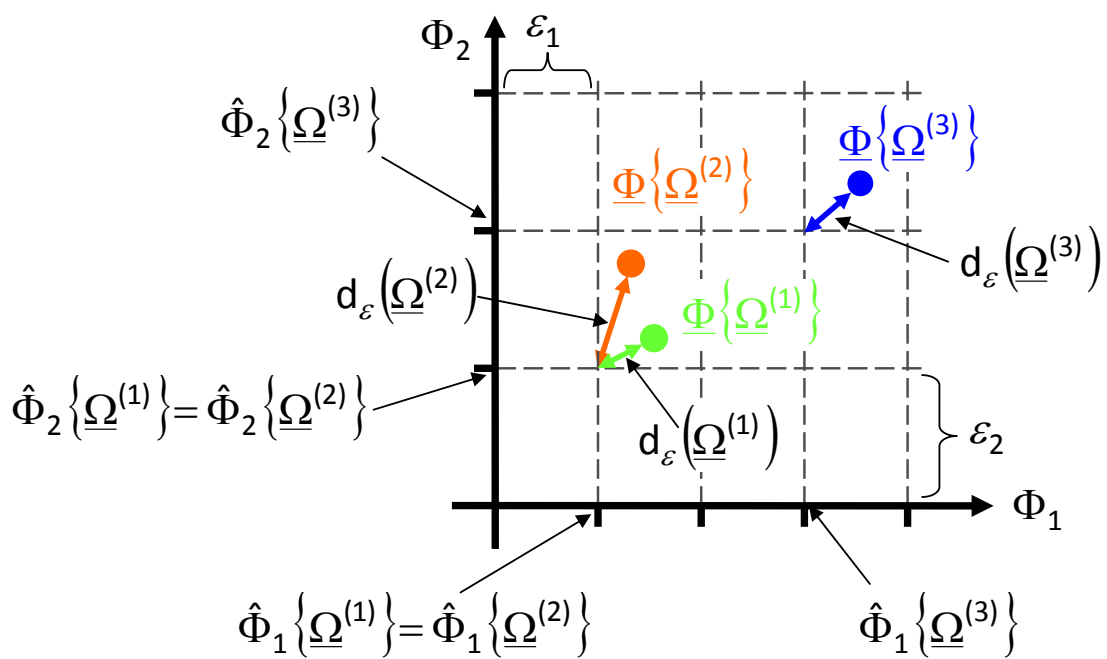


Fig. 1 - P. Rosatti et al., "Multi-Objective System-by-Design for ..."

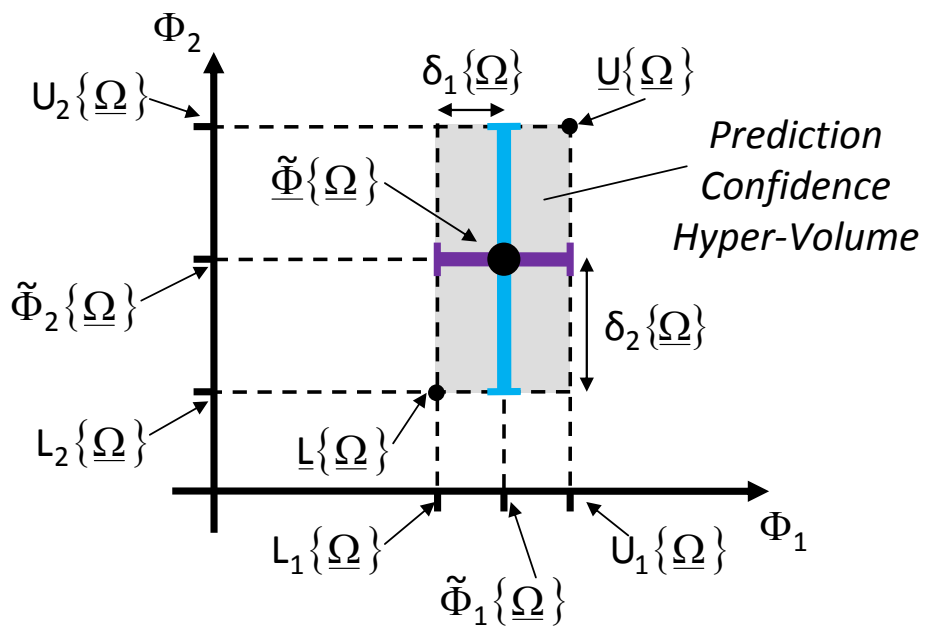


Fig. 2 - P. Rosatti et al., "Multi-Objective System-by-Design for ..."

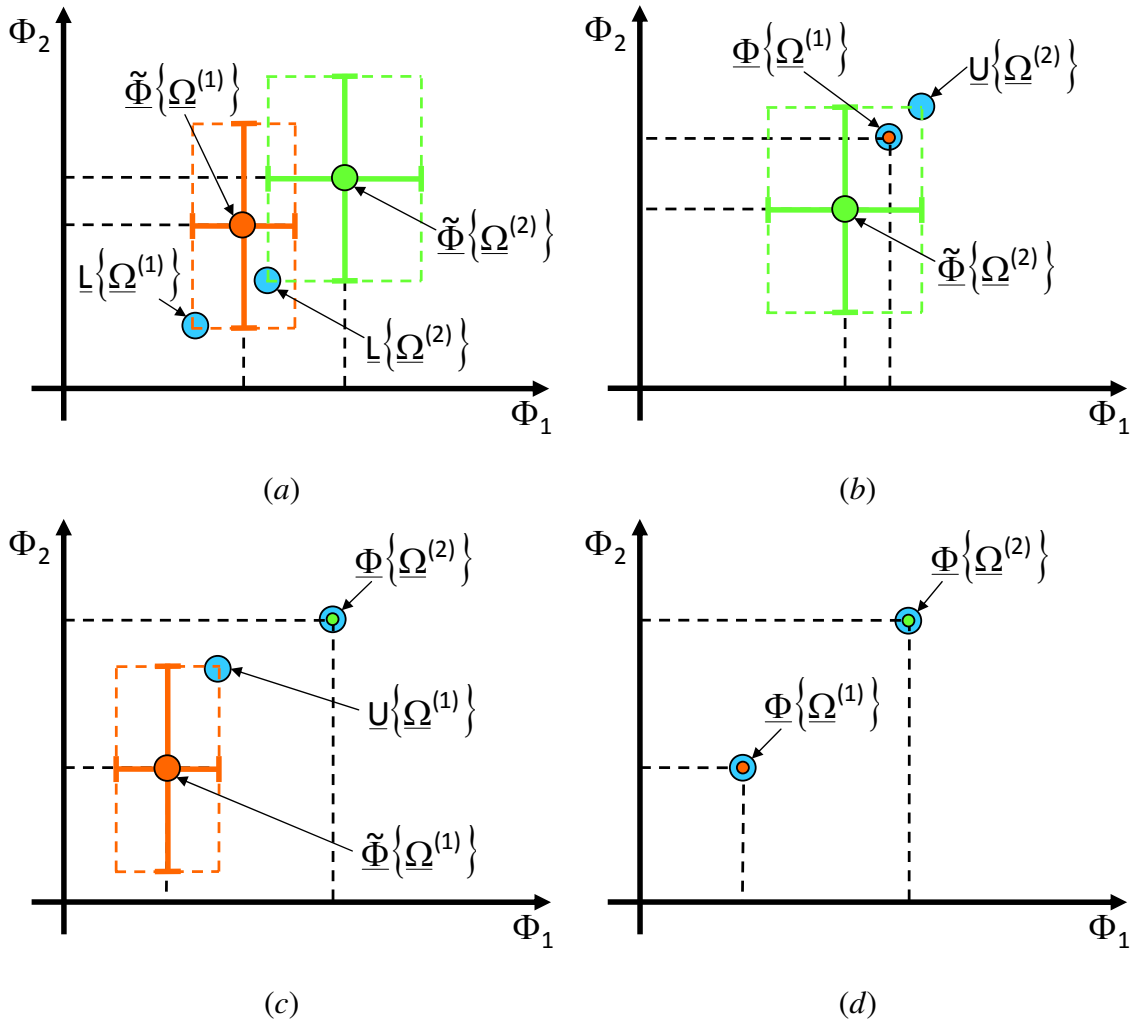


Fig. 3 - P. Rosatti et al., "Multi-Objective System-by-Design for ..."

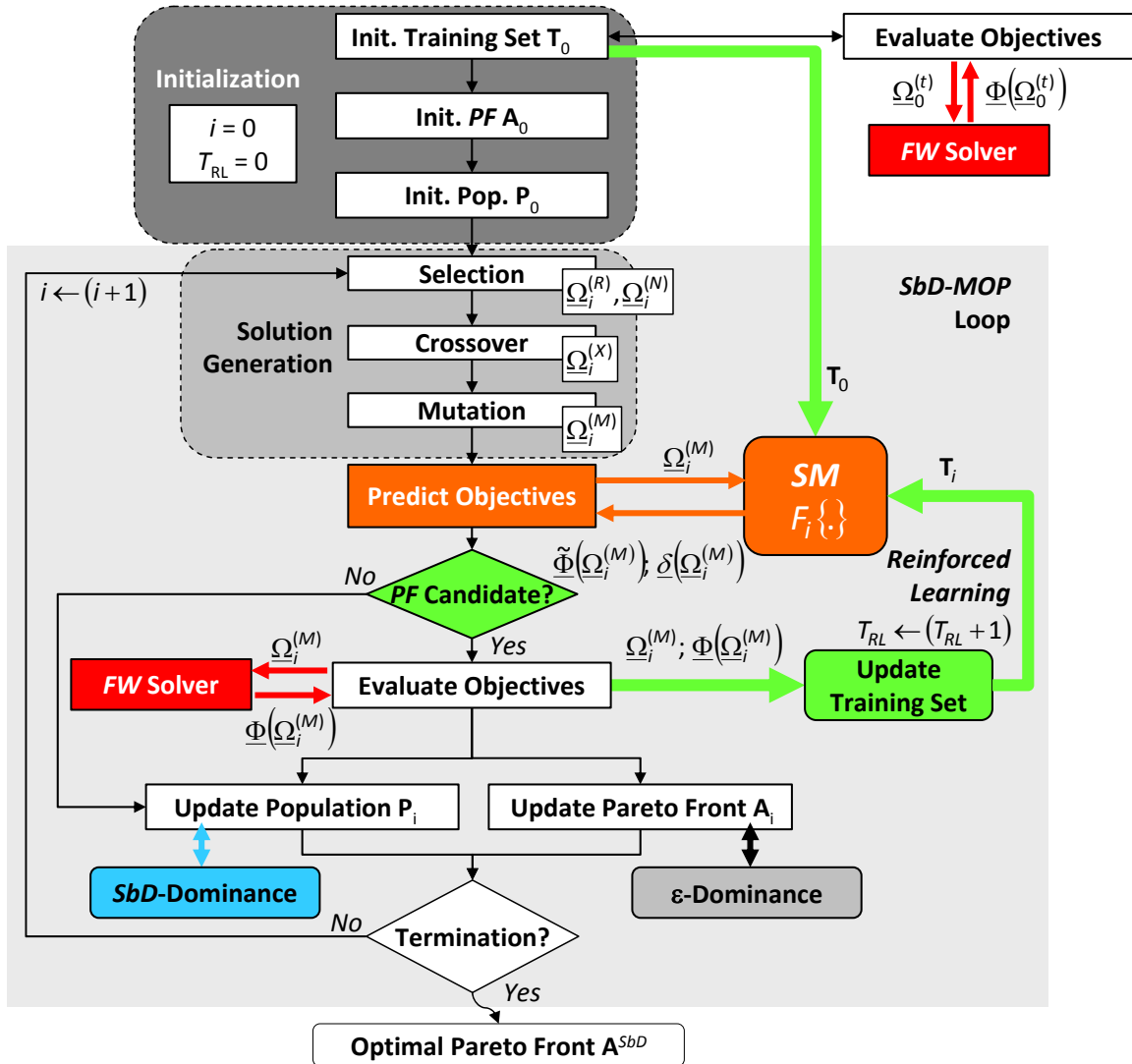


Fig. 4 - P. Rosatti et al., “Multi-Objective System-by-Design for ...”

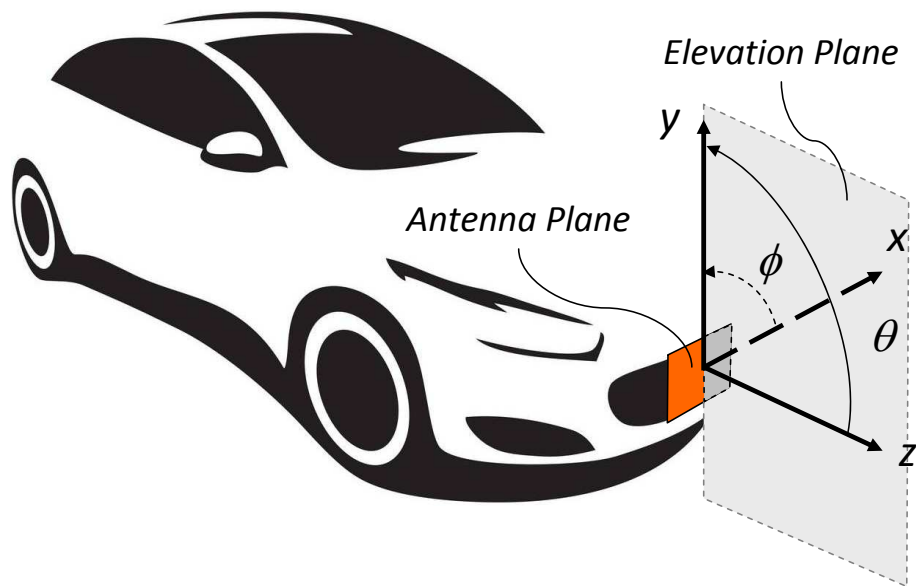
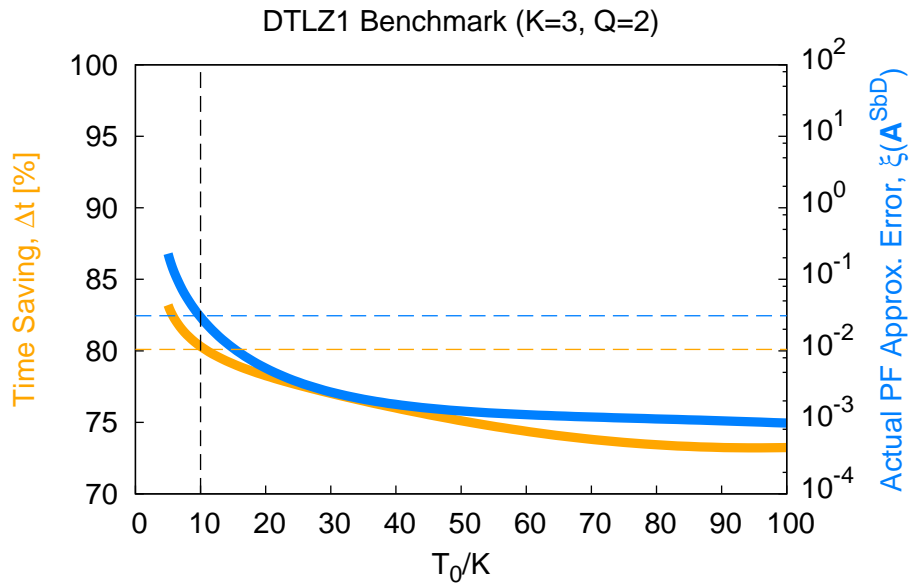
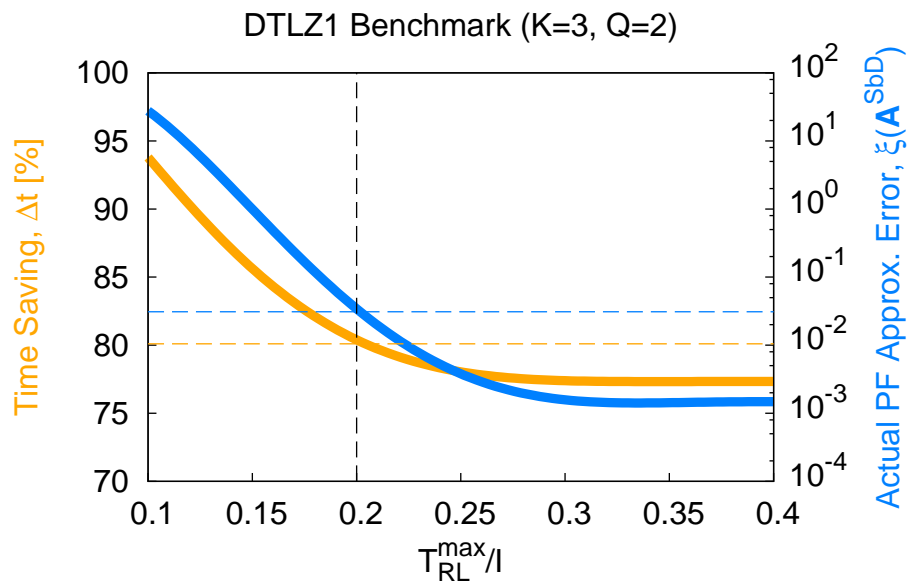


Fig. 5 - P. Rosatti et al., “Multi-Objective System-by-Design for ...”



(a)



(b)

Fig. 6 - P. Rosatti et al., "Multi-Objective System-by-Design for ..."

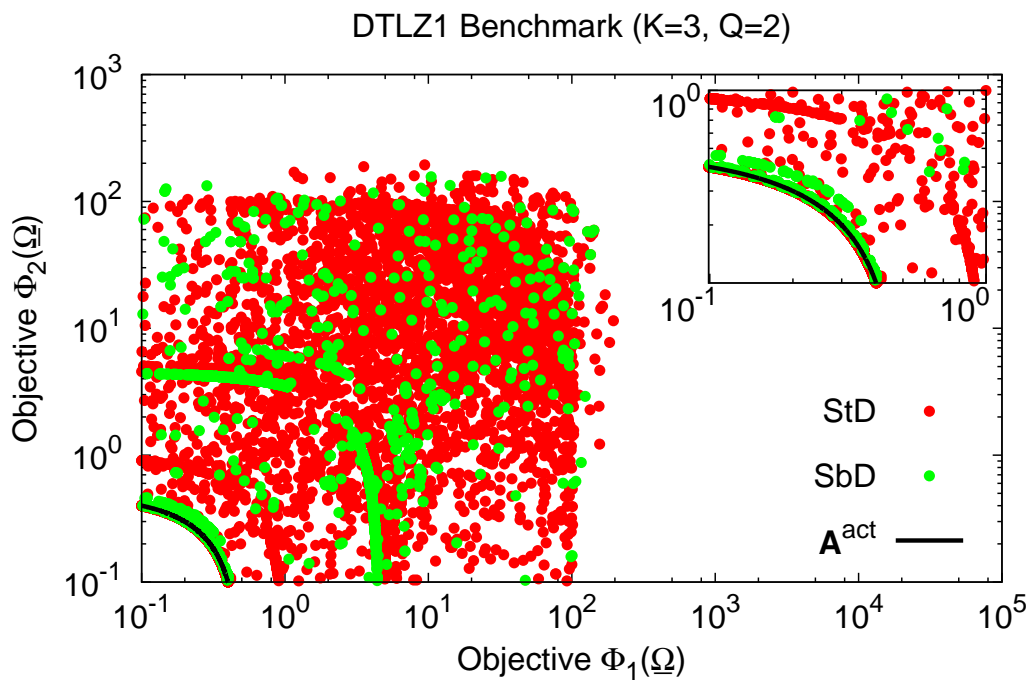
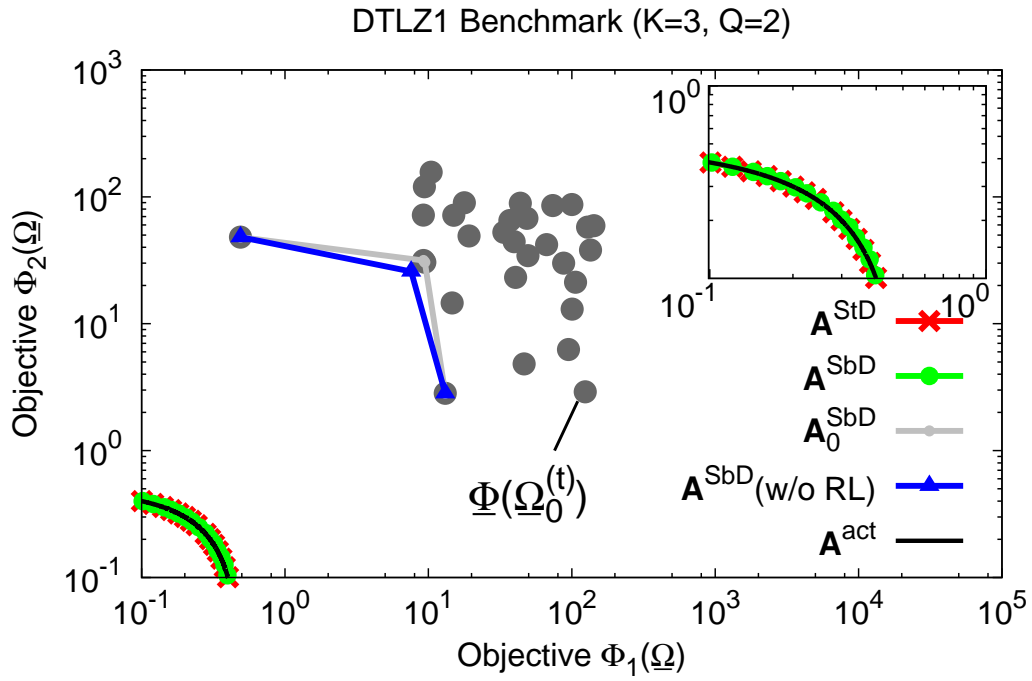


Fig. 7 - P. Rosatti et al., “Multi-Objective System-by-Design for ...”

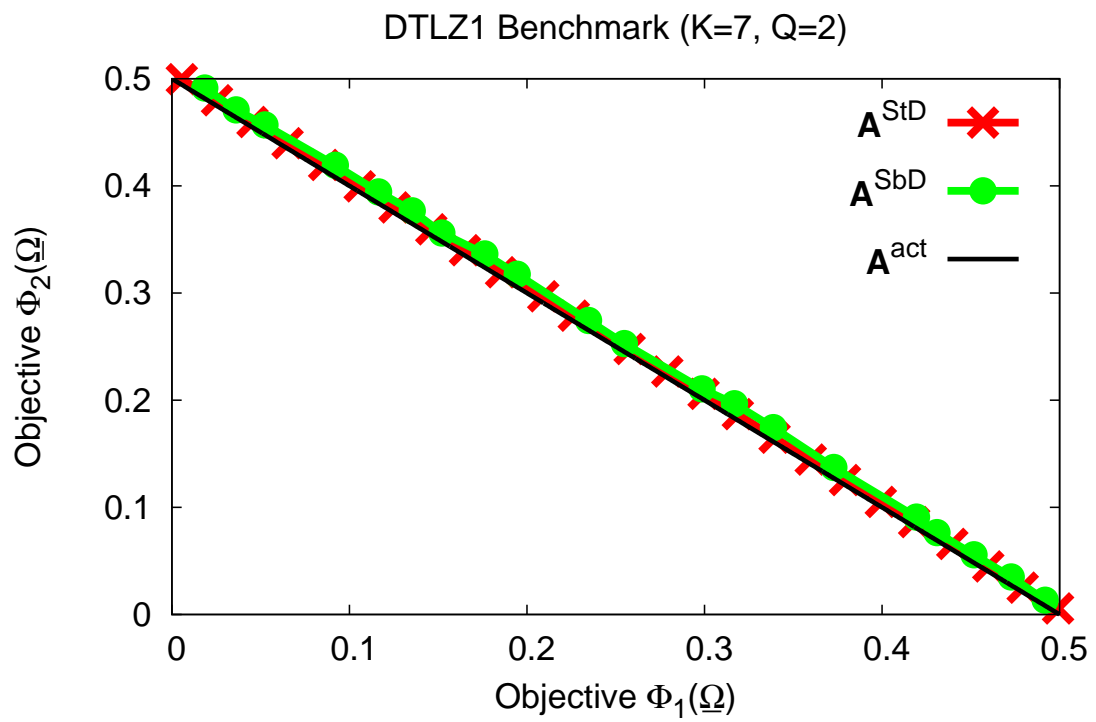


Fig. 8 - P. Rosatti et al., "Multi-Objective System-by-Design for ..."

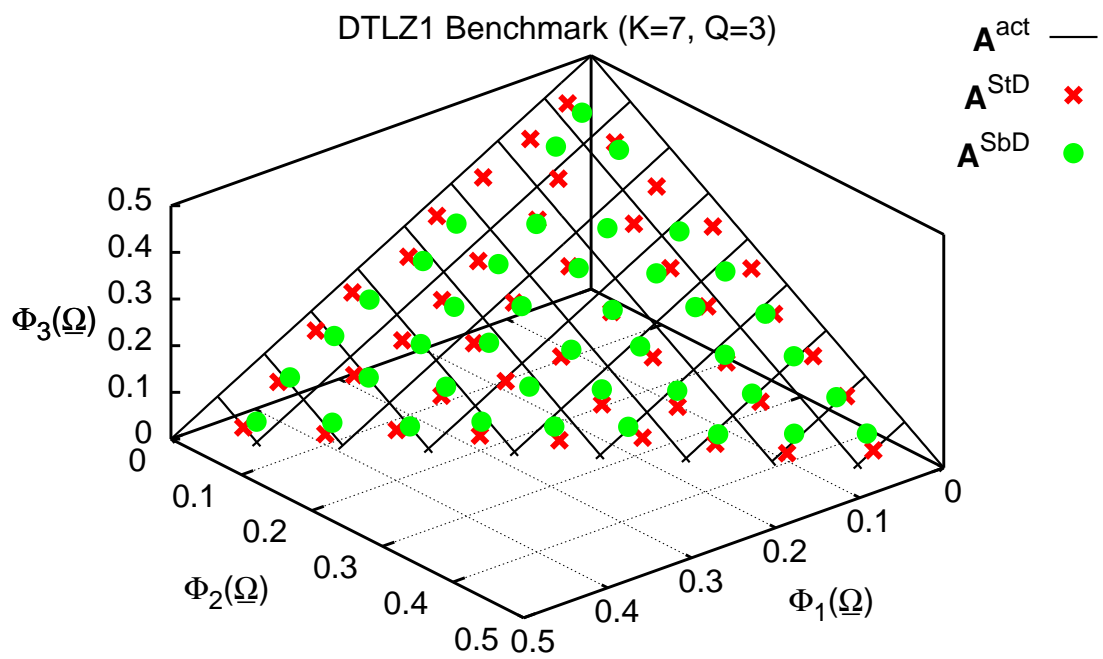


Fig. 9 - P. Rosatti et al., “Multi-Objective System-by-Design for ...”

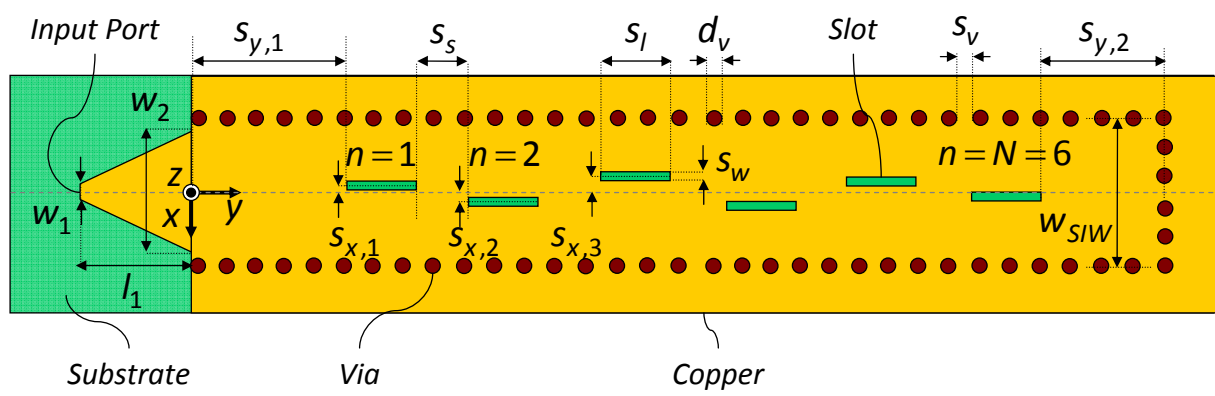
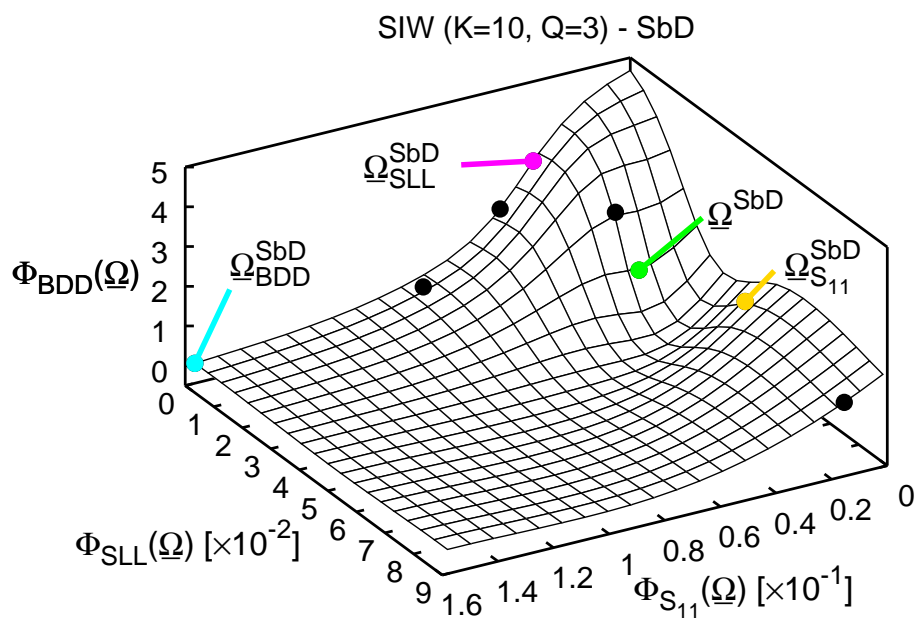
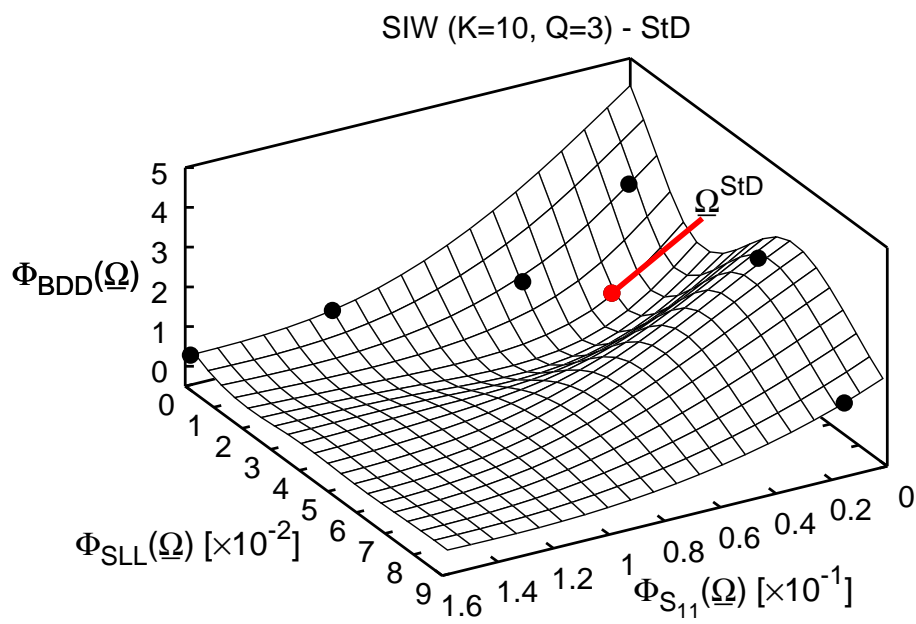


Fig. 10 - P. Rosatti et al., “Multi-Objective System-by-Design for ...”

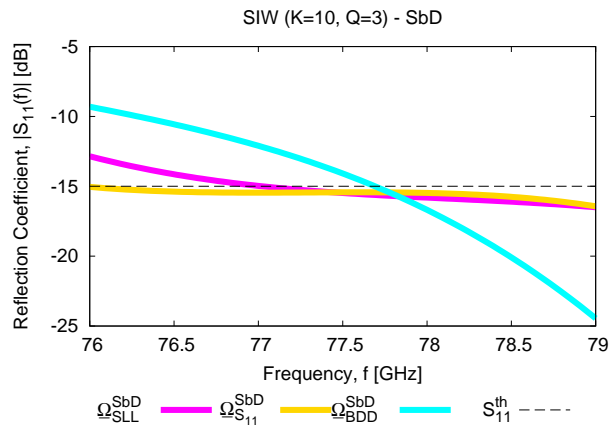


(a)

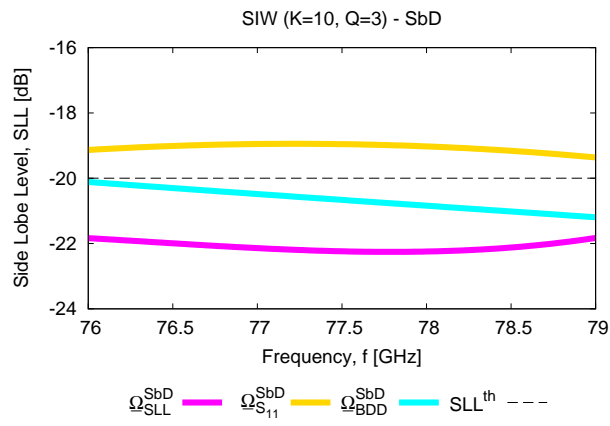


(b)

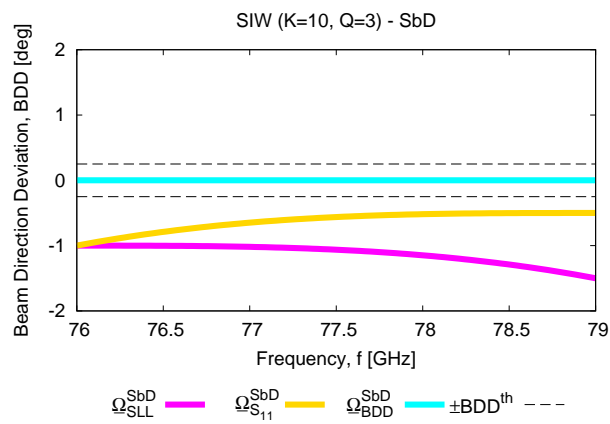
Fig. 11 - P. Rosatti et al., “Multi-Objective System-by-Design for ...”



(a)



(b)



(c)

Fig. 12 - P. Rosatti et al., “Multi-Objective System-by-Design for ...”

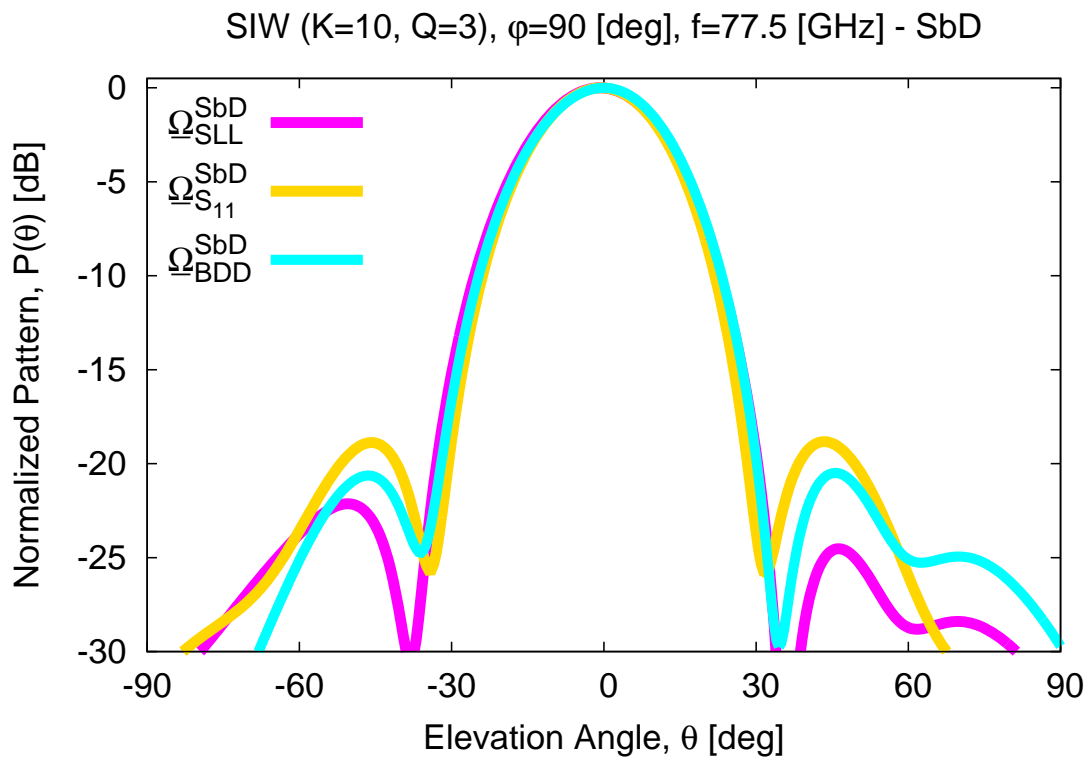
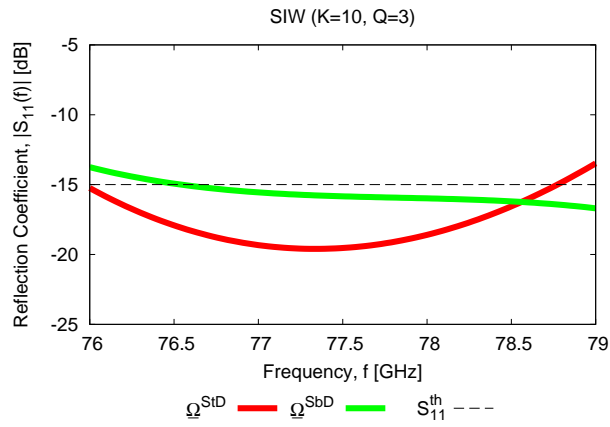
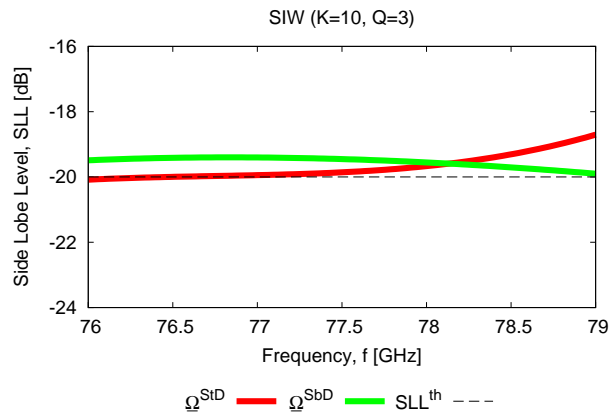


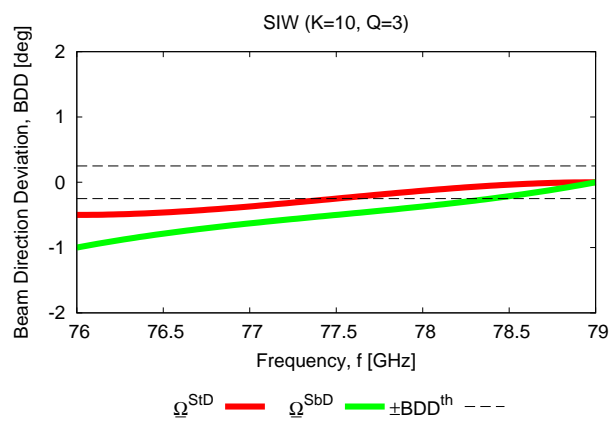
Fig. 13 - P. Rosatti et al., "Multi-Objective System-by-Design for ..."



(a)

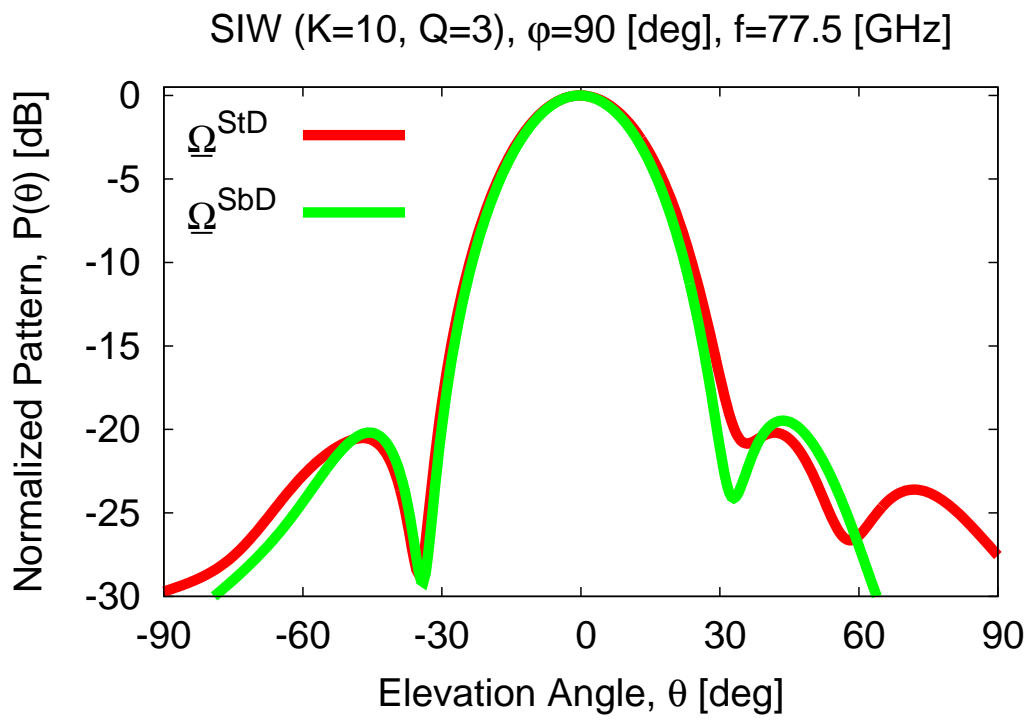


(b)

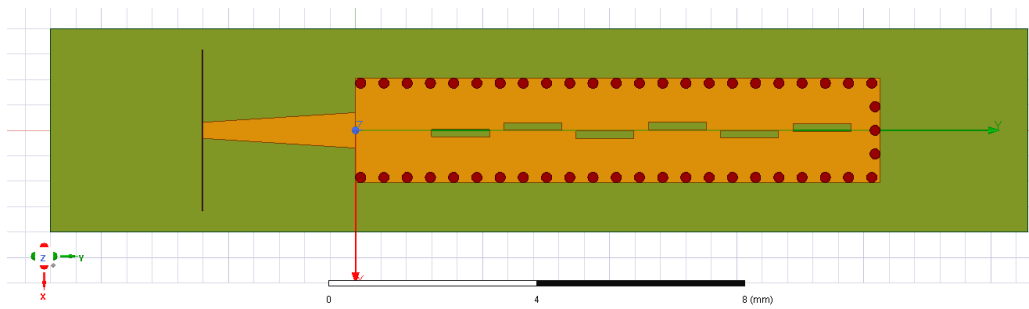


(c)

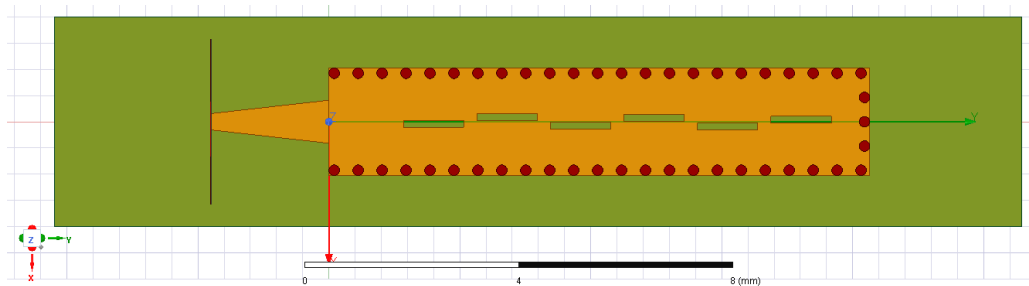
Fig. 14 - P. Rosatti et al., “Multi-Objective System-by-Design for ...”



(a)

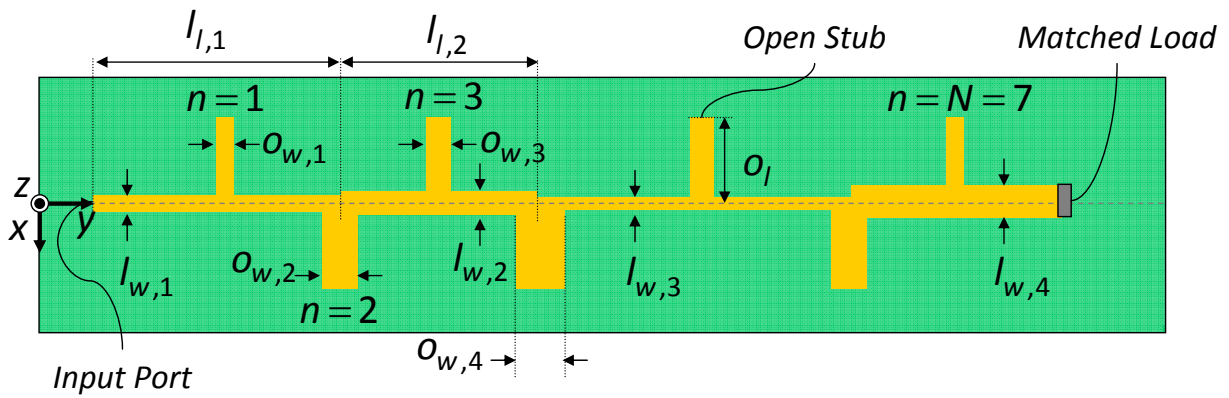


(b)

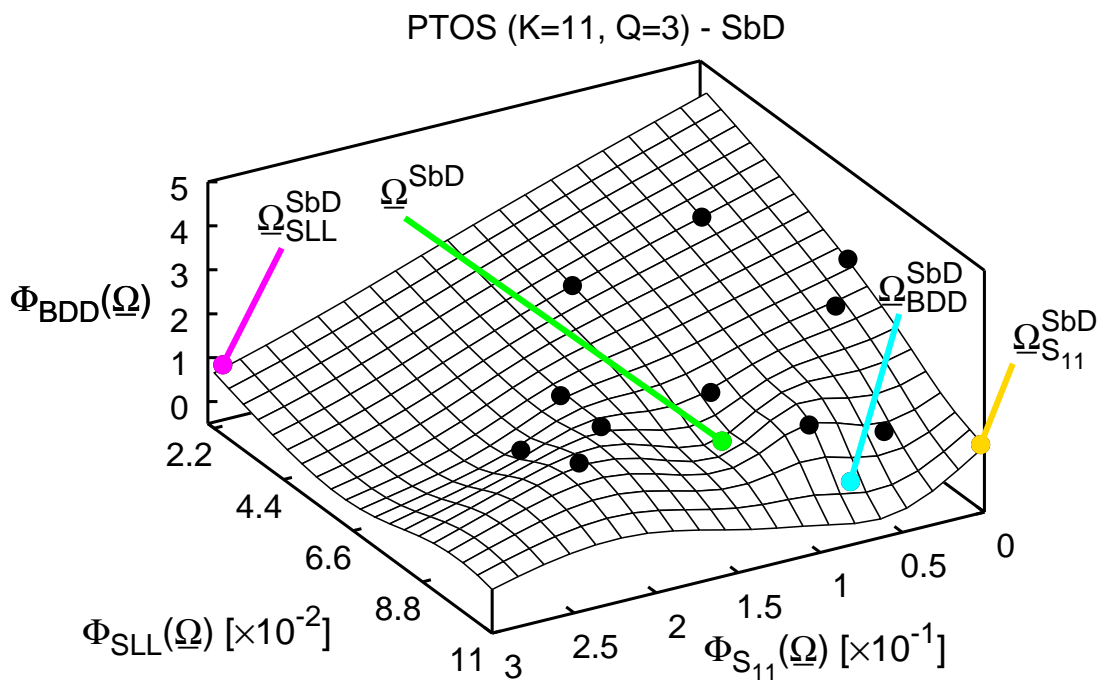


(c)

Fig. 15 - P. Rosatti et al., "Multi-Objective System-by-Design for ..."

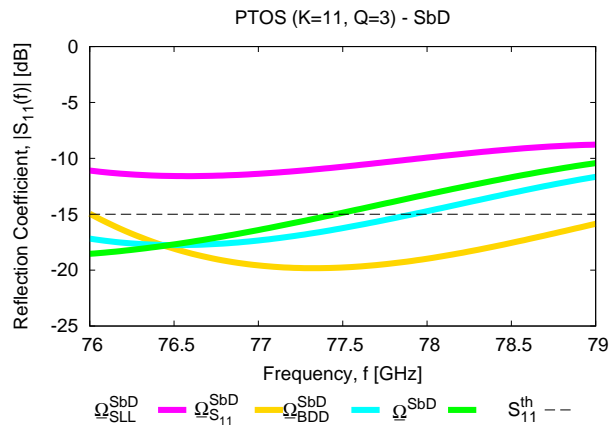


(a)

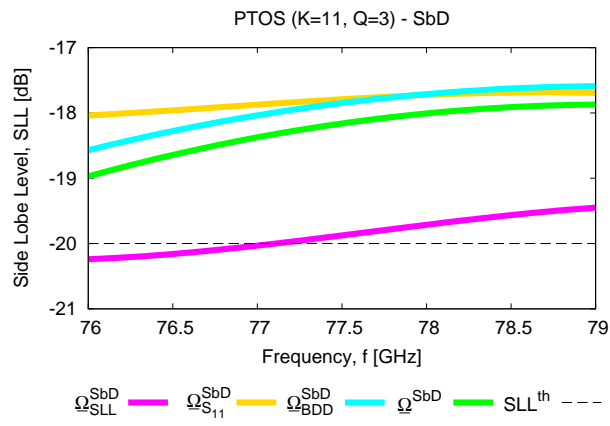


(b)

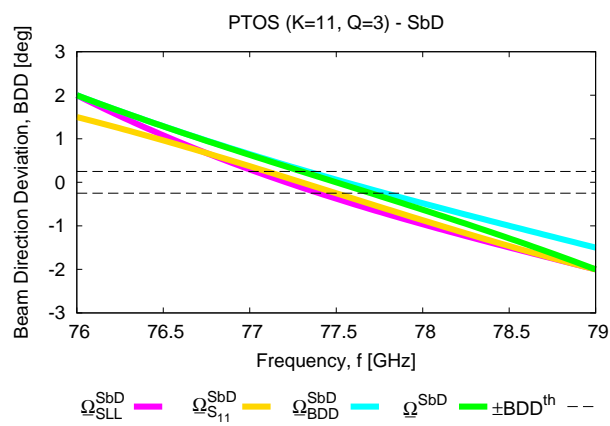
Fig. 16 - P. Rosatti et al., "Multi-Objective System-by-Design for ..."



(a)

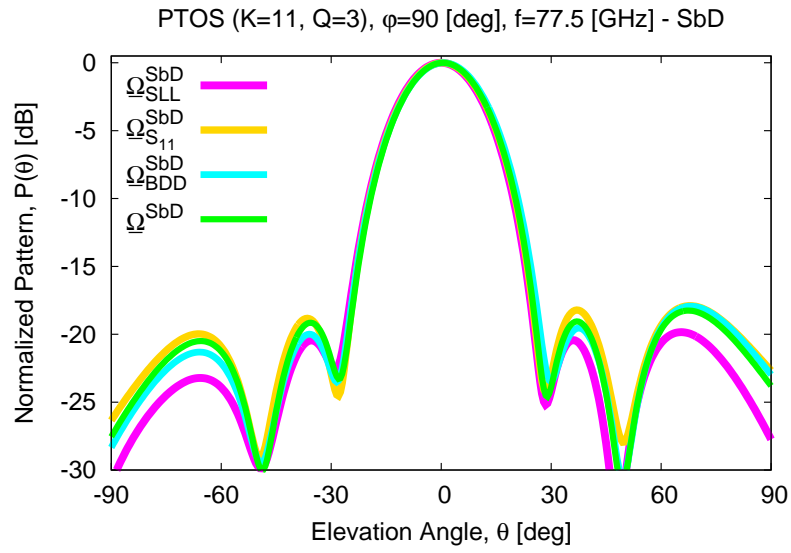


(b)

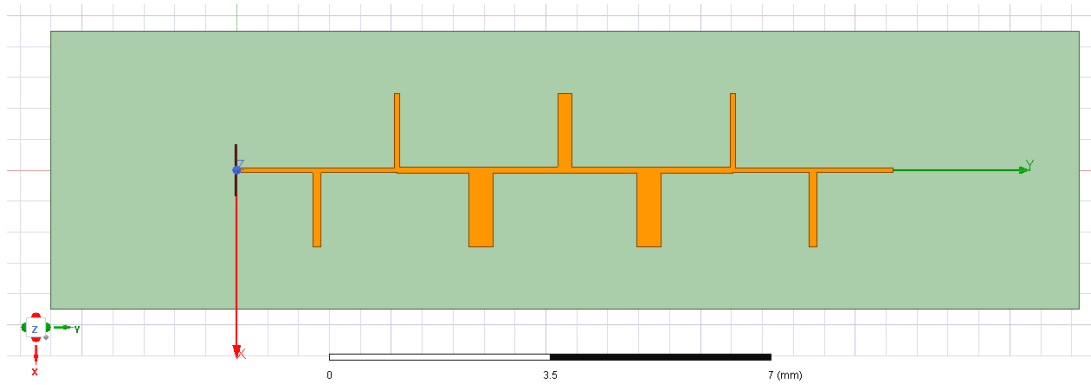


(c)

Fig. 17 - P. Rosatti et al., "Multi-Objective System-by-Design for ..."



(a)



(b)

Fig. 18 - P. Rosatti et al., “Multi-Objective System-by-Design for ...”

	$\tilde{\Phi}(\underline{\Omega}^{(1)})$	$\Phi(\underline{\Omega}^{(1)})$
$\tilde{\Phi}(\underline{\Omega}^{(2)})$	$\left\{ \begin{array}{l} \mathcal{L}_q(\underline{\Omega}^{(1)}) \leq \mathcal{L}_q(\underline{\Omega}^{(2)}) \\ \text{for } q = 1, \dots, Q \\ \exists q \in \{1, \dots, Q\} \\ \text{for which } \mathcal{L}_q(\underline{\Omega}^{(1)}) < \mathcal{L}_q(\underline{\Omega}^{(2)}) \end{array} \right.$ <p style="text-align: center;">[Fig. 3(a)]</p>	$\left\{ \begin{array}{l} \Phi_q(\underline{\Omega}^{(1)}) \leq \mathcal{U}_q(\underline{\Omega}^{(2)}) \\ \text{for } q = 1, \dots, Q \\ \exists q \in \{1, \dots, Q\} \\ \text{for which } \Phi_q(\underline{\Omega}^{(1)}) < \mathcal{U}_q(\underline{\Omega}^{(2)}) \end{array} \right.$ <p style="text-align: center;">[Fig. 3(b)]</p>
$\Phi(\underline{\Omega}^{(2)})$	$\left\{ \begin{array}{l} \mathcal{U}_q(\underline{\Omega}^{(1)}) \leq \Phi_q(\underline{\Omega}^{(2)}) \\ \text{for } q = 1, \dots, Q \\ \exists q \in \{1, \dots, Q\} \\ \text{for which } \mathcal{U}_q(\underline{\Omega}^{(1)}) < \Phi_q(\underline{\Omega}^{(2)}) \end{array} \right.$ <p style="text-align: center;">[Fig. 3(c)]</p>	$\left\{ \begin{array}{l} \Phi_q(\underline{\Omega}^{(1)}) \leq \Phi_q(\underline{\Omega}^{(2)}) \\ \text{for } q = 1, \dots, Q \\ \exists q \in \{1, \dots, Q\} \\ \text{for which } \Phi_q(\underline{\Omega}^{(1)}) < \Phi_q(\underline{\Omega}^{(2)}) \end{array} \right.$ <p style="text-align: center;">[Fig. 3(d)]</p>

Tab. I - P. Rosatti et al., “Multi-Objective System-by-Design for ...”

Condition	$\tilde{\Phi}(\underline{\Omega}_i^{(\mathcal{M})})$	$\Phi(\underline{\Omega}_i^{(\mathcal{M})})$
$\exists \underline{\Omega} \in \mathbf{P}_{i-1} : \underline{\Omega} \prec_{SbD} \underline{\Omega}_i^{(\mathcal{M})}$	$\mathbf{P}_i \leftarrow \mathbf{P}_{i-1}$	$\mathbf{P}_i \leftarrow \mathbf{P}_{i-1}$
$\left\{ \begin{array}{l} \exists \underline{\Omega} \in \mathbf{P}_{i-1}^{pred} : \underline{\Omega}_i^{(\mathcal{M})} \prec_{SbD} \underline{\Omega} \\ \nexists \underline{\Omega}' \in \mathbf{P}_{i-1} : \underline{\Omega}' \prec_{SbD} \underline{\Omega}_i^{(\mathcal{M})} \end{array} \right.$	$\underline{\Omega} \leftarrow \underline{\Omega}_i^{(\mathcal{M})}$	$\underline{\Omega} \leftarrow \underline{\Omega}_i^{(\mathcal{M})}$
$\left\{ \begin{array}{l} \exists \underline{\Omega} \in \mathbf{P}_{i-1}^{sim} : \underline{\Omega}_i^{(\mathcal{M})} \prec_{SbD} \underline{\Omega} \\ \nexists \underline{\Omega}' \in \mathbf{P}_{i-1}^{pred} : \underline{\Omega}' \prec_{SbD} \underline{\Omega}_i^{(\mathcal{M})} \end{array} \right.$	$\underline{\Omega} \leftarrow \underline{\Omega}_i^{(\mathcal{M})}$	$\underline{\Omega} \leftarrow \underline{\Omega}_i^{(\mathcal{M})}$
$\left\{ \begin{array}{l} \nexists \underline{\Omega} \in \mathbf{P}_{i-1} : \underline{\Omega}_i^{(\mathcal{M})} \prec_{SbD} \underline{\Omega} \\ \nexists \underline{\Omega}' \in \mathbf{P}_{i-1} : \underline{\Omega}' \prec_{SbD} \underline{\Omega}_i^{(\mathcal{M})} \\ \mathbf{P}_{i-1}^{pred} \neq \emptyset \end{array} \right.$	$\mathcal{R} \{ \mathbf{P}_{i-1}^{pred} \} \leftarrow \underline{\Omega}_i^{(\mathcal{M})}$	$\mathcal{R} \{ \mathbf{P}_{i-1}^{pred} \} \leftarrow \underline{\Omega}_i^{(\mathcal{M})}$
$\left\{ \begin{array}{l} \nexists \underline{\Omega} \in \mathbf{P}_{i-1} : \underline{\Omega}_i^{(\mathcal{M})} \prec_{SbD} \underline{\Omega} \\ \nexists \underline{\Omega}' \in \mathbf{P}_{i-1} : \underline{\Omega}' \prec_{SbD} \underline{\Omega}_i^{(\mathcal{M})} \\ \mathbf{P}_{i-1}^{pred} = \emptyset \end{array} \right.$	$\mathbf{P}_i \leftarrow \mathbf{P}_{i-1}$	$\mathcal{R} \{ \mathbf{P}_{i-1}^{sim} \} \leftarrow \underline{\Omega}_i^{(\mathcal{M})}$

Tab. II - P. Rosatti et al., “Multi-Objective System-by-Design for ...”

k	DoF	Ω_k^{SbD} [mm] [Fig. 15(b)]	Ω_k^{StD} [mm] [Fig. 15(c)]
1	l_1	2.99	2.24
2	w_2	0.70	0.82
3	$s_{y,1}$	1.50	1.42
4	$s_{y,2}$	0.47	0.63
5	s_s	0.28	0.25
6	s_l	1.14	1.15
7	s_w	0.15	0.13
8	$s_{x,1}$	0.06	0.04
9	$s_{x,2}$	0.08	0.09
10	$s_{x,3}$	0.09	0.07

Tab. III - P. Rosatti et al., “Multi-Objective System-by-Design for ...”

k	DoF	Ω_k^{SbD} [mm] [Fig. 18(b)]
1	$l_{l,1}$	2.59
2	$l_{l,2}$	2.71
3	$l_{w,1}$	0.08
4	$l_{w,2}$	0.11
5	$l_{w,3}$	0.10
6	$l_{w,4}$	0.07
7	$o_{w,1}$	0.14
8	$o_{w,2}$	0.08
9	$o_{w,3}$	0.40
10	$o_{w,4}$	0.24
11	o_l	1.24

Tab. IV - P. Rosatti et al., “Multi-Objective System-by-Design for ...”